https://ntrs.nasa.gov/search.jsp?R=19670007238 2020-03-16T18:44:16+00:00Z

CR 73060

4-06-66-12 • JULY 1966

4-06-66-12

CONVECTIVE AND RADIATIVE HEAT TRANSFER TO AN ABLATING BODY

by

H. HOSHIZAKI and L. E. LASHER

GPO PRICE $ _____

CFSTI PRICE(S) $ _____

Hard copy (HC) 3.00

Microfiche (MF) 1.30

ff 653 July 65

N67 16567 (ACCESSION NUMBER) (THRU)

79 (PAGES) 1 (CODE)

NASA CR-73060 (NASA CR OR TMX OR AD NUMBER) 33 (CATEGORY)

FACILITY FORM 602

CONVECTIVE AND RADIATIVE HEAT TRANSFER TO AN ABLATING BODY

by

H. Hoshizaki and L. E. Lasher

4-06-66-12

July 1966

Final Report, Part I,
Prepared Under NAS 7-386

LOCKHEED PALO ALTO RESEARCH LABORATORY
LOCKHEED MISSILES & SPACE COMPANY
A GROUP DIVISION OF LOCKHEED AIRCRAFT CORPORATION

FOREWORD

The work described in this report was completed for the National Aeronautics and Space Administration Headquarters, under the terms and specifications of Contract NAS 7-386, issued through NASA Resident Office - JPL, 4800 Oak Grove Drive, Pasadena, California.

The work was performed in the Aerospace Sciences Laboratory, R. Capiaux, Manager, of the Lockheed Palo Alto Research Laboratory.

ABSTRACT

The convective and radiative heat transfer to entry vehicles protected by ablation heat shields is investigated. The effect of mass injection, radiative emission and absorption, radiation cooling, and coupling between convection and radiation are included in the analysis. The absorption coefficients of the shock layer gas, including the pyrolysis products species, are determined as a function of particle number density, temperature, and radiation frequency. An integral method is used to obtain an approximate solution to the momentum equation. This approximate solution yields the velocity profiles which are used to solve the species continuity and energy equations. The latter two equations are solved numerically by means of a finite difference type method. Typical results for the shock layer structure and convective and radiative heating are presented. They indicate that the absorption of the molecules added by ablation does not significantly affect the radiative heat flux to the surface; this was true for mass injection rates up to 5% of the free stream mass flux.

ACKNOWLEDGMENTS

The authors would like to express their sincere appreciation to K. H. Wilson and H. L. Schick of the Laboratory for their helpful discussions and suggestions during the course of the work described in this report. Particular thanks are extended to H. R. Kirch for her many contributions in IBM code revisions, programming, and suggestions on the numerical analysis.

CONTENTS

ILLUSTRATIONS

NOMENCLATURE

a_i	velocity profile coefficients
B_ν	Planckian radiation intensity
C_j	mass fraction of jth species
$\tilde{C}_i$	elemental mass fraction of ith element
C_p	total specific heat at constant pressure
$\bar{C}_p$	frozen specific heat at constant pressure
C_v	specific heat at constant volume
c	light velocity
D_j	effective binary diffusion coefficient of species j
$\tilde{D}_i$	effective elemental binary diffusion coefficient
E'	radiant emission per unit time per unit volume
E_o^o	internal energy at 0^oK
$\mathcal{E}_n$	exponential function
F^o	Gibbs free energy function
f	velocity function, u/u_δ; also molecular band f-number
H	total enthalpy
h	static enthalpy, also Planck constant
h_j	static enthalpy of jth species, including enthalpy of formation.
I_ν	spectral radiation intensity, energy per unit time, area, solid angle, and frequency.

I_o	mass conservation integral
I_1	momentum-integral
k	total thermal conductivity, also Boltzmann constant
k_R	reaction thermal conductivity
k_{TR}	translational thermal conductivity
k_{INT}	internal thermal conductivity
$\bar{k}$	frozen thermal conductivity
K_p	equilibrium constant at constant pressure
L	Loschmidt number
Le_j	Lewis number of jth species $Le_j = \frac{\rho D_j C_p}{k}$
M_j	molecular weight of species j
$M_{i,j}$	defined as number of grams of elements per gram of species j.
$\bar{M}$	molecular weight of mixture
$\dot{m}$	mass flux of pyrolysis products
$\dot{M}_R$	mass flux associated with surface reactions
N	number density
p_j	partial pressure of jth species
P	static pressure
Pr	total Prandtl number, $Pr = C_p\mu/k$
$\overline{Pr}$	frozen Prandtl number, $Pr = \bar{C}_p\mu/\bar{k}$
$\dot{q}_c$	convective energy flux
$\dot{q}_r$	radiative energy flux
R	body radius

R	perfect gas constant
Re	Reynolds number, $\rho_{\delta,o} U_\infty R/\mu_{\delta,o}$
r	body radius measured from body centerline
S	entropy
$Sc_{\tilde{i}}$	Schmidt number of element i $\nu/D_{\tilde{i}}$
T	temperature
U	free-stream velocity
$\bar{U}$	velocity in 10^4 fps
u	velocity component parallel to body, also non-dimensional frequency, $h\nu/kT$
v	velocity component normal to surface
$\dot{\omega}_j$	net rate of production of species j
x,y	body-oriented coordinate system
$\alpha_{\tilde{i}}$	number of grams of element $\tilde{i}$ per gram of pyrolysis product.
δ	shock detachment distance
$\tilde{\delta}$	transformed shock detachment distance
ϵ	difference between body and shock angle
η	Dorodnitzyn variable
θ	body angle, also kT
$\varkappa$	body curvature
$\tilde{\varkappa}$	$1 + \varkappa y$
$\varkappa_\nu$	volumetric absorption coefficient, cm^{-1}
λ_R	radiation mean free path

μ	dynamic viscosity
$\bar{\Omega}^{(2,2)}$	collision integral for viscosity
$\bar{\Omega}^{(1,1)}$	collision integral for diffusion
ν	kinematic viscosity, also frequency
ξ	nondimensional surface distance, x/R, also Biberman function.
ρ	density
$\bar{\rho}$	density ratio across shock, ρ_∞/ρ_ξ
σ^*	effective cross section, $\sigma^* = \kappa_\nu/N$
τ_ν	monochromatic optical thickness
ϕ	shock angle
ϕ_{ji}	parameter used in computing transport properties of a mixture.
ω	vorticity, also solid angle

Subscripts

CN	cyano molecule
CO	carbon monoxide molecule
C_2H, C_3H, C_4H, C_2H_2	hydrocarbon molecules
CHN	hydrogen cyanide molecule
$\bar{e}$	electron
H_2	hydrogen molecule
H	hydrogen atom

H^+	hydrogen ion
i	ith element
j	jth chemical species
N_2	nitrogen molecule
N	nitrogen atom
N^+	nitrogen ion
O_2	oxygen molecule
O	oxygen atom
O^+	oxygen ion
t	total
w	wall quantities
δ	quantities immediately behind shock
∞	free-stream condition
0	stagnation point

Superscript

	dimensional quantity

Section 1

INTRODUCTION

The heating encountered by a superorbital vehicle entering a planetary atmosphere is so severe that ablating heat shields are required. The injection of pyrolysis products into the shock layer can greatly complicate its structure by chemically reacting with the air species. In addition, surface mass transfer can have a very significant effect on both the convective and radiative heat transfer. For entry velocities in the neighborhood of 50,000 fps, the ablation rates can be large enough to blow the viscous layer off the wall. When this occurs, the convective heating is reduced essentially to zero and the only mode of heating is radiation. The ablation vapor layer will absorb the radiant flux incident upon it and thus reduce the radiation to the surface. The absorption of radiant energy depends on the spectral distribution of the incident radiation and the absorption coefficient of the species present in the vapor layer. Hence, the evaluation of the radiant energy transfer to the surface requires knowledge of the shock-layer temperature profile, species number density distribution, and species absorption coefficient. The shock-layer properties are in turn dependent on the radiant energy transfer so that the problem is coupled.

The objective of this investigation is to examine this coupled problem in detail. This paper is an extension of the analysis presented in Ref. (1) to include a detailed examination of the effect of ablation. In the analysis nylon-phenolic is picked as a typical ablator and 20 species are considered, viz. C, C^+, C_2, H, H^+, H_2, N, N^+, N_2, O, O^+, O_2, $\bar{e}$, CN, CO, C_2H, C_3H, C_4H, C_2H_2 and CHN. The shock-layer gas is assumed to be in chemical equilibrium. The diffusion of a particular species is assumed to occur as if the gas were a binary mixture, one component being the particular species in question,

with the other component representing the remaining species.

The radiant energy transfer in the air-pyrolysis product mixture is evaluated spectrally. For atomic and ionic species, only the continuum absorption coefficients are employed. Line absorption coefficients are neglected. For the molecular species, the smeared band model is adopted for the purpose of evaluating the molecular line absorption coefficients.

An important physical mechanism in the shock-layer flow is the coupling between the inviscid and viscous regions created by radiant energy transfer. This coupling is taken into account by considering the entire flow region between the shock and the body simultaneously. The advantage of this approach is that it eliminates the necessity of matching the frequency-dependent radiation flux at the inviscid-viscid interface. The conservation equations are first simplified by means of the thin shock-layer approximations. The momentum equation is solved by the Karman-Pohlhausen integral method while the diffusion and energy equations are solved by a finite difference type method. The solution yields the convective and radiative heating as well as complete details of the shock-layer structure.

Section 2

ANALYSIS

2.1 GOVERNING EQUATIONS

In this analysis a direct solution to the radiating, viscous, blunt-body problem is sought. The conservation equations are first simplified by assuming the shock layer to be thin; i.e., $\delta/R \ll 1$. In addition, the thickness of the viscous region is taken to be of the same order of magnitude as the shock-layer thickness. Since the shock-detachment distance is $O(\bar{\rho})$ and the thickness of the viscous region is $O(1/\sqrt{Re})$, we have for a viscous shock layer, $\bar{\rho} \sim 1/\sqrt{Re}$. The thin shock-layer equations are also valid when the viscous region is confined to a narrow region near the wall ($\bar{\rho} \gg 1/\sqrt{Re}$).

The approximate equations valid for thin shock layers can be obtained from the conservation equations (Ref. 2) by neglecting all terms of $O(\bar{\rho}^2)$ and higher. The body-oriented coordinate system used in this analysis is shown in Fig. 1. Carrying out the order-of-magnitude analysis results in the following equations valid to $O(\bar{\rho})$.

x-momentum

$$\rho' u' \frac{\partial u'}{\partial x'} + \tilde{\kappa}\rho' v' \frac{\partial u'}{\partial y'} + \kappa'\rho' u' v' = - \frac{\partial P'}{\partial x'} - \frac{1}{\tilde{\kappa} r'} \frac{\partial}{\partial y'} \left[r' u' \tilde{\kappa}^2 \frac{\partial \mu'}{\partial y'} \right] + \frac{\tilde{\kappa}}{r'} \frac{\partial}{\partial y'} \left[\frac{r'}{\tilde{\kappa}} \frac{\partial (\tilde{\kappa}\mu' u')}{\partial y'} \right] \tag{1}$$

y-momentum

$$\rho' u' \frac{\partial v'}{\partial x'} + \rho' v' \frac{\partial v'}{\partial y'} - \frac{\kappa'\rho' u'^2}{\tilde{\kappa}} = - \frac{\partial P'}{\partial y'} + \frac{4}{3} \frac{\partial}{\partial y'} \left[\frac{\mu'}{r'} \frac{\partial (r' u')}{\partial x'} + \mu' \frac{\partial v'}{\partial y'} \right]$$

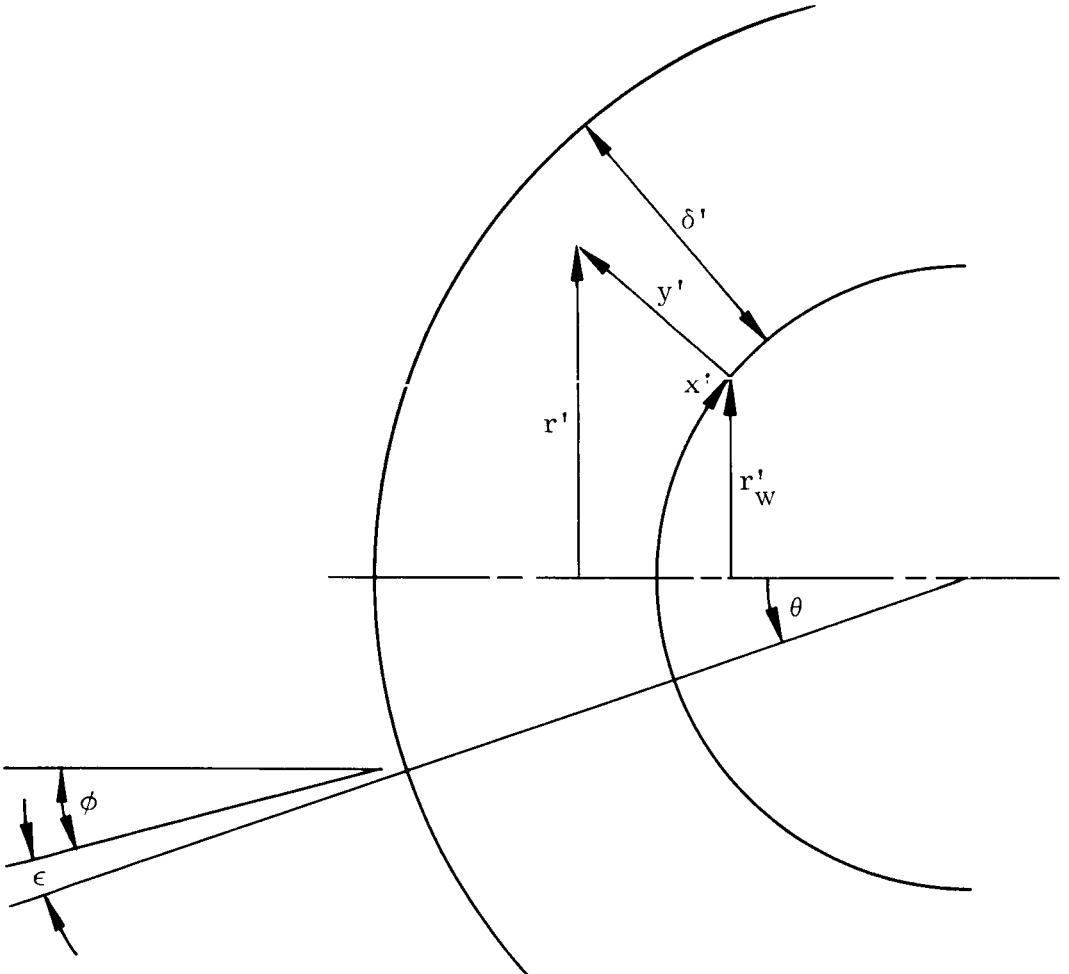

$$\tan \epsilon = \frac{d\delta'}{(1 + \kappa'\delta')\, dx'}$$

$$\delta' = \int_0^{x'} (1 + \kappa'\delta') \tan \epsilon \, dx' + \delta'_o$$

$$r' = r'_w + y' \sin \theta$$

Fig. 1 Body-Oriented Coordinate System

$$+ \frac{\partial}{\partial y'} \left(u' \frac{\partial \mu'}{\partial x'} \right) + \frac{\partial u'}{\partial y'} \frac{\partial \mu'}{\partial x'} - \frac{1}{r'} \frac{\partial \mu'}{\partial y'} \frac{\partial (r'u')}{\partial x'} - \frac{1}{r'} \frac{\partial}{\partial x'} \left[r' \frac{\partial (\mu' u')}{\partial y'} \right] \quad (2)$$

Global continuity

$$\frac{\partial}{\partial x'} (r'\rho'u') + \frac{\partial}{\partial y'} (r'\tilde{\kappa}\rho'v') = 0 \quad (3)$$

jth species continuity

$$r'\rho'u' \frac{\partial C_j}{\partial x'} + r'\rho'v'\tilde{\kappa}' \frac{\partial C_j}{\partial y'} = \frac{\partial}{\partial y'} \left[r'\tilde{\kappa}\rho' D'_j \frac{\partial C_j}{\partial y'} \right] + \dot{\omega}_j \quad (4)$$

Energy

$$\frac{\rho'u'}{\tilde{\kappa}} \frac{\partial h'}{\partial x'} + \rho'v' \frac{\partial h'}{\partial y'} = u' \frac{\partial P'}{\partial x'} + v' \frac{\partial P'}{\partial y'} + \frac{1}{\tilde{\kappa} r'} \frac{\partial}{\partial y'} \left[r'\tilde{\kappa} \{ \bar{k}' \frac{\partial T'}{\partial y'} + \sum \rho' h'_j D'_j \frac{\partial C_j}{\partial y'} \} \right] + \mu' \left[\tilde{\kappa} \frac{\partial}{\partial y'} \left(\frac{u'}{\tilde{\kappa}'} \right) \right]^2 - E' \quad (5)$$

For terms of $O(\bar{\rho})$ in the above equations we have set $\tilde{\kappa} = 1$ and $r = r(x)$ to be consistent with our order-of-magnitude approximation. These approximations to the higher order terms are made throughout the analysis. These equations differ slightly from the thin shock-layer equations presented by Hayes and Probstein (Ref. 3) since our analysis is not restricted to stagnation-point flows.

The simplified shock layer equations, Eqs. (1-5) form a set of parabolic partial differential equations. In principal, with initial data given at the stagnation point, i.e., along the line $x = 0$, these equations can be integrated about the body. Such an approach requires the simultaneous development of the shock boundary by integrating the geometric relation (cf. Fig. 1),

$$d\delta'/dx' = (1 + \kappa'\delta')\tan \epsilon$$

We have followed an alternative approach in which an initial iterative estimate on the shock curvature $d\phi/dx$ is specified for all x. Note that by twice integrating the shock curvature, the shock-detachment distance is determined to within an arbitrary constant. The arbitrary constant is taken from the stagnation-point solution for $\delta(x = 0)$. The technique of prescribing the shock boundary has more significance than a practical method of solution. Since the governing equations are parabolic with characteristics given by x = const., then the problem is mathematically not well-set in terms of initial data prescribed along the characteristic, x = 0. The specification of boundary data along the "strips" defined by the body and shock leads to a well set problem and one which is stable to numerical integration.

At the stagnation point, symmetry conditions provide all but one boundary condition necessary to determine a solution. The remaining boundary condition is either the stagnation-point shock curvature or shock-detachment distance. In the present analysis the unknown boundary condition is supplied by assuming the shock is concentric to the body at the stagnation point, i.e., $d\phi/dx = d\theta/dx$. The iterative method mentioned above (see also Sec. 4 Numerical Method) for determining the shock shape for $x > 0$ serves only as a means for obtaining the solution which corresponds to the assumed initial condition at the stagnation point. It does not yield any information about the accuracy of the assumed initial condition. Hence, the solutions are dependent on the assumed initial condition.

The radiation term E' in the energy equation specifies the net emission or absorption of radiant energy per unit volume per unit time. It is calculated assuming the shock layer is locally one-dimensional. That is, for any value of x, temperature and density gradients in the x direction at all points across the shock layer are neglected insofar as radiation transport is concerned. In addition, the geometric approximation is made that the shock-layer geometry is that of an infinite plane slab.

It is clear that without the one-dimensional approximation the radiation transport calculation is much more difficult to perform. More significantly, the parabolic character of the thin shock-layer equations is destroyed as influence can now be propagated upstream via the radiation field. The approximation of replacing the shock-layer geometry by an infinite plane slab requires, for optically thin shock layers, that the shock-layer thickness be small relative to the local radius of curvature, i.e., $\delta/R \ll 1$. For optically thick shock layers the requirement for the plane slab approximation is that the mean free path for radiation λ_R be small compared to the local radius of curvature, i.e., $\lambda_R/R \ll 1$.

Hence, the plane slab approximation becomes more accurate in the important spectral ranges when the shock layer is optically thick. Indeed, Kennet and Strack (Ref. 4) show that for optical depth unity, the plane slab approximation is in error by only 5% for an isothermal spherical shock layer. Concerning the approximation of one-dimensional temperature and density fields, Koh (Ref. 5) has investigated the effects of the non-isothermal temperature in the radiation flux at the stagnation point of a sphere and found only a 3% difference from an isothermal solution when the shock layer has an optical depth of unity. Hence, the one-dimensional plane-parallel slab model can be used to obtain quantitatively valid results.

Except for the locally one-dimensional treatment, the radiation term is evaluated in an exact manner. No approximations restricting the analysis to optically thin or optically thick shock layers are made. Instead a full integral treatment of the emission and absorption processes is made. Moreover, the radiation transport is performed in terms of a detailed spectral analysis using realistic absorption coefficients. The spectral transport solution shows that gray gas approximations using a Planck mean opacity produce results which are in error by as much as an order of magnitude (Ref. 6).

The radiation flux divergence can be expressed as

$$E' = \nabla \cdot \vec{q}_r = - \int_0^\infty \int_{\omega=4\pi} \kappa_\nu (I_\nu - B_\nu) d\omega d\nu \tag{6}$$

In Eq. (6), κ_ν is the volumetric (spectral) absorption coefficient; I_ν is the local radiation intensity; B_ν is the equilibrium (i.e., Planckian) radiation intensity.

Solving for the intensity under the one-dimensional approximation and performing the integration over solid angle indicated by Eq. (6) leads to the following expression for the flux divergence (Ref. 7).

$$-E' = 2\pi \int_0^\infty \kappa_\nu(t) \left\{ \int_0^{\tau_\nu} B_\nu[T(t_\nu)]\, \mathcal{E}_1(\tau_\nu - t_\nu) dt_\nu \right. \tag{7}$$

$$\left. + \int_{\tau_\nu}^{\tau_{\nu s}} B_\nu [T(t_\nu)]\, \mathcal{E}_1(t_\nu - \tau_\nu) dt_\nu - 2B_\nu[T(\tau_\nu)] \right\} d\nu$$

where τ_ν is the optical depth at frequency ν,

$$\tau_\nu = \int_0^{y'} \kappa_\nu(y'') dy'' \tag{8}$$

B_ν is the spectral Planckian intensity,

$$B_\nu = \frac{2h\nu^3}{c^2} \frac{1}{\exp(h\nu/kT) - 1} \tag{9}$$

$\mathcal{E}_n(t)$ is the exponential-integral of order n,

$$\mathcal{E}_n(t) = \int_0^\infty \frac{\exp(-tz)}{z^n} dz \tag{10}$$

In arriving at Eq. (7) it has been assumed that the medium outside the shock wave neither emits, absorbs, or reflects radiant energy and the body surface acts as a perfect absorber and does not reradiate. The quadratures in Eq. (7), for a given shock layer temperature distribution are evaluated numerically using the spectral absorption coefficients described in Sec. 3.

2.2 INTEGRATION OF MOMENTUM EQUATION

In this analysis, solutions to the momentum equation are obtained in an approximate manner by means of an integral method. The velocity profiles resulting from this approximate solution are then used to solve the species continuity and energy equations by means of a modified finite difference method (Ref. 8). The justification for this method of solution rests on the fact that the momentum equation is weakly coupled to the species continuity and energy equation. Approximate velocity and profiles can result in accurate species concentration and total enthalpy profiles if the species continuity and energy equation are solved by finite differences or a similar method.

In carrying out the integral method of solution, the momentum equation is integrated across the shock layer to obtain an integro-differential equation in one independent variable. The integrals are evaluated by assuming that the velocity profile in the shock layer can be represented by suitable polynomials. Before the x-momentum equation is integrated across the shock layer, the viscous terms can be manipulated into a form which is more convenient for integration. Carrying out the manipulation results in

$$\rho' u' \frac{\partial u'}{\partial x'} + \kappa \rho' v' \frac{\partial u'}{\partial y'} + \kappa' \rho' u' v' = - \frac{\partial P'}{\partial x'} + \frac{1}{\tilde{\kappa}} \left(\frac{r'_w}{r'} \right) \frac{\partial}{\partial y'} \left[\tilde{\kappa}^2 \left(\frac{r'}{r'_w} \right) \mu' \frac{\partial u'}{\partial y'} - \kappa' \mu' u' \right] \tag{11}$$

The integration of the x-momentum equations follows closely the work of Maslen and Moeckel (Ref. 9), where additional details of the integration technique are presented. The y-momentum equation is used in the integration of the x-momentum to rewrite the pressure gradient term in a form suitable for integration. For this purpose, the y-momentum is reduced to

$$\varkappa' \rho' u'^2 = \frac{\partial P'}{\partial y'} \tag{12}$$

since the pressure gradient terms are higher order terms. The terms which have been neglected in Eq. (2) are $O(\bar{\rho}^2)$ with respect to the x-momentum equation.

In the analysis to follow, the variables are now nondimensionalized in the following manner:

$$u = \frac{u'}{U'_\infty} \qquad \xi = \frac{x'}{R'} \qquad \delta = \frac{\delta'}{R'} \qquad (\rho v)_w = \frac{(\rho' v')_w}{\rho_\infty U_\infty}$$

$$v = \frac{v'}{U'_\infty} \qquad y = \frac{y'}{R'} \qquad \tilde{\delta} = \frac{\tilde{\delta}'}{R'} \qquad h_\delta = \frac{h'_\delta}{H'_\delta}$$

$$E = \frac{E'R'}{\rho'(U'_\infty)^3} \qquad \rho = \frac{\rho'}{\rho'_{\delta,o}} \qquad \mu = \frac{\mu'}{\mu'_{\delta,o}} \qquad H'_\delta = \frac{1}{2} U'^2_\infty$$

$$\varkappa = \varkappa' R' \qquad H = \frac{H'}{H'_\delta} \qquad P = \frac{P'}{\rho'_\infty U'^2_\infty}$$

$$\tilde{\varkappa} = 1 + \varkappa y \qquad h = \frac{h'}{h'_\delta} \qquad r = \frac{r'}{R'}$$

The compressibility effects can be reduced significantly by introducing the Dorodnitzyn variable defined by

$$\eta = \frac{\int_o^{y'} (r'/r'_w)\, \rho' dy'}{\int_o^{\delta} (r'/r'_w)\, \rho' dy} = \frac{\int_o^{y'} (r'/r'_w)\, \rho' dy}{\tilde{\delta}} \tag{13}$$

Integration of the momentum equation across the shock layer and transformation into the η, ξ variables results in the following integro-differential equations.

momentum

$$\frac{dI_1}{d\xi} + \left[\frac{2}{u_\delta} \frac{du_\delta}{d\xi} + \frac{1}{r_w} \frac{dr_w}{d\xi} (1 + \delta\varkappa) \right] I_1 - \left(1 + \frac{\delta \sin\theta}{r_w} \right) \rho_\delta \frac{d\delta}{d\xi}$$

$$- \frac{d\varkappa}{d\xi} \delta^2 \int_o^1 \left(f^2 \int_o^\eta \frac{d\bar{\eta}}{\rho} \right) d\eta + \left[1 + \delta \left(\frac{\sin\theta}{r_w} + 2\varkappa \right) \right] \frac{v_\delta \rho_\delta}{u_\delta}$$

$$= - \frac{\delta\tilde{\rho}}{u_\delta^2} \left(\frac{\partial P}{\partial \xi} \right)_\delta + \frac{1}{\delta u_\delta Re} \left[\left\{ 1 + 2\delta \left(\frac{\sin\theta}{r_w} + \varkappa \right) \right\} (\rho\mu)_\delta f'(1) - \mu_\delta \delta\varkappa \right.$$

$$\left. - (\rho\mu)_w f'(0) \right] \tag{14}$$

where

$$I_1 = \tilde{\delta} \int_o^1 f^2 \, d\eta$$

$$f = u/u_\delta \tag{15}$$

In addition, the following approximation was used to obtain the second term in the momentum equation:

$$\tilde{\kappa}_\delta I_1 \approx \tilde{\delta} \int_o^1 \tilde{\kappa} f^2 \, d\eta$$

The velocity profile is assumed to be representable by a polynomial in η where the coefficients are functions of the streamwise variable ξ. The coefficients are determined from boundary conditions applied at the wall and immediately behind the shock. The shock-boundary conditions are the usual Rankine-Hugoniot relations which can be expressed as follows:

$$u_\delta = \sin \phi \sin \epsilon + \bar{\rho} \cos \phi \sin \epsilon \tag{16}$$

$$v_\delta = \sin \phi \sin \epsilon - \bar{\rho} \cos \phi \cos \epsilon \tag{17}$$

$$P_\delta = (1-\bar{\rho}) \cos^2 \phi \tag{18}$$

A fifth-order polynomial is used to represent the velocity profile.

$$\frac{u}{u_\delta} = f = \sum_{i-o}^{5} a_i \eta^i \tag{19}$$

Sufficient boundary conditions are specified so that the coefficient a_i can be expressed in terms of known quantities evaluated at the wall and behind the shock wave, and the shock-detachment distance. The integrated momentum equation is used to determine the shock-detachment distance. The six boundary conditions used to determine the velocity profile coefficients are as follows:

(1) $u = 0, \eta = 0$

(2) $u = u_\delta, \eta = 1$

(3) $v = v_\delta, \eta = 1$

(4) Momentum equation evaluated at the wall

(5) $\omega = \omega_\delta$, $\eta = 1$

(6) $f'' = 0$, $\eta = 1$

Primes denote differentiation with respect to η.

2.3 SPECIES CONTINUITY EQUATION

The continuity equations (Eq. (4)) for the numerous species considered in this analysis are not solved explicitly. Instead we adopt the elemental approach (Ref. 10) in which the species continuity equation for each element is satisfied. Once the elemental concentration is known, the concentration of the molecular, atomic and ionic species are determined by means of an equilibrium thermodynamic calculation (Sec. 3).

In the present analysis, four elements are considered, viz., oxygen, nitrogen, carbon and hydrogen. The elemental concentrations are related to the molecular, atomic and ionic species by the following relations.

$$\tilde{C_O} = C_O + C_{O+} + C_{O_2} + M_{O,CO} C_{CO} \tag{20}$$

$$\tilde{C_N} = C_N + C_{N+} + C_{N_2} + M_{N,CN}\, C_{CN} + M_{N,CHN}\, C_{CHN} \tag{21}$$

$$\begin{aligned}\tilde{C_C} = {} & C_C + C_{C+} + C_{C_2} + M_{C,CN}\, C_{CN} + M_{C,CO}\, C_{CO} \\ & + M_{C,C_2H}\, C_{C_2H} + M_{C,C_3H}\, C_{C_3H} + M_{C,C_4H}\, C_{C_4H} + M_{C,C_2H_2}\, C_{C_2H_2} \\ & + M_{C,CHN}\, C_{CHN}\end{aligned} \tag{22}$$

$$C_{\tilde{H}} = C_H + C_{H^+} + C_{H_2} + M_{H,C_2H}\, C_{C_2H} + M_{H,C_3H}\, C_{C_3H}$$
$$+ M_{H,C_4H}\, C_{C_4H} + M_{H,C_2H_2}\, C_{C_2H_2} + M_{H,CHN}\, C_{CHN} \qquad (23)$$

The coefficients $M_{i,j}$ are equal to the number of grams of element i per gram of species j.

The continuity equation for each of the elements can be obtained by multiplying the continuity equation for species j (Eq. 4) by $M_{i,j}$ and summing over all species j which contain the element i. The j species which contain i elements are as follows:

TABLE I

i element	j species
$C_{\tilde{O}}$:	O, O+, O_2, CO
$C_{\tilde{N}}$:	N, N+, N_2, CN, CHN
$C_{\tilde{C}}$:	C, C+, C_2, CN, CO, C_2H, C_3H, C_4H, C_2H_2, CHN
$C_{\tilde{H}}$:	H, H+, H_2, C_2H, C_3H, C_4H, C_2H_2, CHN

Carrying out the summation and by using Eqs. (20-23), the elemental species continuity equation can be written as (one for each element i)

$$r'\rho'u' \frac{\partial C_{\tilde{i}}}{\partial x'} + r'\rho'v' \tilde{\kappa} \frac{\partial C_{\tilde{i}}}{\partial y'} = \frac{\partial}{\partial y'} \left[r'\tilde{\kappa}\, \rho' \sum_j D_j M'_{ij} \frac{\partial C_j}{\partial y'} \right] \qquad (24)$$

since, barring nuclear transformations, $\sum_j M_{i,j} \dot{\omega}_j = 0$. Since we have that $\sum_{\tilde{i}} C_{\tilde{i}} = 1$, only three equations of the type Eq. (24) are independent. The three elements chosen to be described by Eq. (24) were O, N, and C. Now it is necessary to assume that the effective binary diffusion coefficient is the same for

LOCKHEED PALO ALTO RESEARCH LABORATORY
LOCKHEED MISSILES & SPACE COMPANY
A GROUP DIVISION OF LOCKHEED AIRCRAFT CORPORATION

each species. This assumption is necessary to derive a species continuity equation for element and to assure global mass conservation. For example, for the element oxygen, it is assumed that the effective binary diffusion coefficient of O, O^+, O_2 and CO are identical. Since the diffusion coefficients are inversely proportional to the square root of the reduced molecular weights, (i.e. $\sqrt{M_i + M_j/M_i M_j}$ this approximation is acceptable as long as the molecular weights of the species are similar. One can then choose an average diffusion coefficient which is representative of the actual diffusion coefficients. When light elements are present, such as hydrogen in the present case, this approximation is quite poor. However, since one purpose of the present analysis is to develop a method for investigating the effect of ablation products on the radiative and convective heat transfer, the approximation is conservative. This is the case because the concentration of hydrogen near the wall will be overestimated since it will not appear to diffuse as fast as it should.

As an alternative to using a binary diffusion coefficient we can define an elemental diffusion coefficient as

$$\tilde{D_i'} = \frac{\sum D_j' M_{i,j} \frac{\partial C_j}{\partial y'}}{\sum M_{i,j} \frac{\partial C_j}{\partial y'}}$$

An a posteriori check may be made on an assumed $\tilde{D_i'}$ after the diffusion equations are solved. A thermo-chemical equilibrium calculation is performed to supply the $\frac{\partial C_j}{\partial y'}$ needed for this check. It is possible in this manner to set up an iteration procedure for the specification of $\tilde{D_i'}$. This procedure can become quite complex and we resort to the approximation discussed above to simplify the analysis. With this approximation, Eq. (24) can be written as

$$r'\rho'u' \frac{\partial \tilde{C_i}}{\partial x'} + r'\rho'v' \tilde{\nu}' \frac{\partial \tilde{C_i}}{\partial y'} = \frac{\partial}{\partial y'} \left[r'\tilde{\nu}\rho' D_i' \frac{\partial \tilde{C_i}}{\partial y'} \right] \qquad (25)$$

Two boundary conditions are necessary to define the species concentration variation across the shock layer. The first boundary condition is that the injected species concentration is zero at the shock. The second boundary condition is obtained from a mass balance at the wall. The total mass flux at the surface is

$$\rho' v' = \alpha_{\tilde{O}} \dot{m}' + \alpha_{\tilde{H}} \dot{m}' + \alpha_{\tilde{N}} \dot{m}' + \alpha_{\tilde{C}} \dot{m}' + \dot{M}_{R'} \tag{26}$$

where $\dot{m}'$ is the mass flux of the pyrolysis product*, $\alpha_{\tilde{O}}$ is the number of grams of oxygen per gram of pyrolysis product (similar definitions for $\alpha_{\tilde{H}}$, $\alpha_{\tilde{N}}$ and $\alpha_{\tilde{C}}$) and $\dot{M}'_R$ is the mass flux associated with surface reactions. We will consider charring ablators where the char is pure carbon. Only two surface reactions will be considered and these reactions will be assumed to produce carbon monoxide. The surface reactions considered are:

$$C_{(s)} + O_{(g)} \xrightarrow{\bar{k}_1} CO_{(g)} \tag{27}$$

$$C_{(s)} + 1/2\ O_{2(g)} \xrightarrow{\bar{k}_2} CO_{(g)}$$

so that

$$\dot{M}'_R = \rho' M'_C\, T'^{1/2} \left(k'_1 \frac{C_O}{M'_O} + k'_2 \frac{C_{O_2}}{M'_O} e^{-k''_2/T'} \right) \tag{28}$$

Mass balances at the surface for the elements yield

$$C_{\tilde{O}} (\rho' v') - \rho' D_{\tilde{O}}' \frac{\partial C_{\tilde{O}}}{\partial y'} = \alpha_{\tilde{O}} \dot{m}' \tag{29}$$

*The mass flux of the pyrolysis product is assumed to be a known quantity. In general, it can be obtained from an energy balance at the surface.

$$C_{\tilde{N}}(\rho' v') - \rho' D_{\tilde{N}}' \frac{\partial C_{\tilde{N}}}{\partial y'} = \alpha_{\tilde{N}} \dot{m}' \tag{30}$$

$$C_{\tilde{C}}(\rho' v') - \rho' D_{\tilde{C}}' \frac{\partial C_{\tilde{C}}}{\partial y'} = \alpha_{\tilde{C}} \dot{m}' + \dot{M}_R' \tag{31}$$

In terms of the transformed variables ξ, η, the elemental species continuity equation is

$$\frac{\partial}{\partial \eta}\left[\rho\mu \left(\frac{r}{r_w}\right)^2 \frac{\tilde{\kappa}}{Sc_i} \frac{\partial C_{\tilde{i}}}{\partial \eta}\right] + \tilde{\delta}\, Re u_\delta \left[\frac{\partial I_o}{\partial \xi} + I_o \left(\frac{1}{u_\delta}\frac{du_\delta}{d\xi} + \frac{1}{r_w}\frac{\partial r_w}{\partial \xi}\right)\right.$$

$$\left. - (\rho v)_w \frac{\bar{\rho}}{u_\delta}\right] \frac{\partial C_{\tilde{i}}}{\partial \eta} = Re\, \tilde{\delta}\, u_\delta\, f \frac{\partial C_{\tilde{i}}}{\partial \xi} \tag{32}$$

where the mass flux, normal to the surface, was replaced by the following expression obtained by integrating the global continuity equation.

$$\tilde{\delta} f \frac{\partial \eta}{\partial \xi} + \left(\frac{r}{r_w}\right) \varkappa \frac{\rho v}{u_\delta} = - \frac{\partial I_o}{\partial \xi} - I_o \frac{\partial/\partial \xi (u_\delta r_w)}{u_\delta r_w} + \frac{(\rho v)_w}{u_\delta} \tag{33}$$

The quantity $I_o(\eta)$ is defined by

$$I_o = \tilde{\delta} \int_o^\eta f d\eta \tag{34}$$

Eq. (32) is of the form

$$\frac{\partial}{\partial \eta}\left[\frac{1}{F_1}\frac{\partial C_{\tilde{i}}}{\partial \eta}\right] + \left[\frac{1}{F_1}\frac{\partial C_{\tilde{i}}}{\partial \eta}\right] F_2 = L_1 \tag{35}$$

The solution for $C_{\tilde{i}}$ is

$$C_{\tilde{i}} = \int_o^{\eta} \left[F_1 \int_o^{\eta} L_1 e^{-\int_{\eta'}^{\eta} F_2 d\eta'} d\eta + F_1 C_1 e^{-\int_o^{\eta} F_2 d\eta} \right] d\eta + C_2 \qquad (36)$$

where the constants of integration (C_1 and C_2) are determined from the two boundary conditions discussed previously.

2.4 ENERGY EQUATION

It is somewhat more convenient in carrying out the numerical solution to rewrite the energy equation in terms of total enthalpy. Combining the momentum equations (Eqs. (11), (12)) with the energy equation written in terms of the static enthalpy (Eq. (5)) results in

$$\frac{\rho' u'}{\tilde{\kappa}} \frac{\partial H'}{\partial x'} + \rho' v' \frac{\partial H'}{\partial y'} = \frac{1}{\tilde{\kappa}} \left(\frac{r'}{r'}_W\right) \left\{ \frac{\partial}{\partial y'} \left[\tilde{\kappa}^2 \frac{r'}{r_w'} \mu' \frac{\partial (u'^2/2)}{\partial y'} \right] - \kappa' \frac{\partial}{\partial y'} (\mu' u'^2) \right\} \qquad (37)$$

$$+ \frac{1}{\tilde{\kappa}} \frac{r'_W}{r'} \frac{\partial}{\partial y'} \left[\frac{r'}{r_w'} \tilde{\kappa} \left(\bar{k}' \frac{\partial T'}{\partial y} + \rho' \sum_j D_j' h_j' \frac{\partial C_j}{\partial y'} \right) \right] - E'$$

The diffusion term, which represents the transport of enthalpy by diffusion, requires discussion. Although one can argue that the diffusion coefficient for each species is similar, the enthalpy for each species, h_j', varies widely for the species considered. Hence, it becomes necessary to evaluate the enthalpy transported by diffusion by each species j.

The evaluation of the species concentration gradients presents some difficulty. The gradients can be written as

$$\frac{\partial C_j}{\partial y'}\frac{(T', P', C_{\tilde{i}})}{} = \frac{\partial C_j}{\partial T'}\frac{\partial T'}{\partial y'} + \sum_{\tilde{i}}^{4} \frac{\partial C_j}{\partial C_{\tilde{i}}}\frac{\partial C_{\tilde{i}}}{\partial y'} \tag{38}$$

where we have neglected the effect of pressure on the grounds that the temperature gradients are much larger than pressure gradients.

The quantity $\partial C_j/\partial T'$ can be determined from equilibrium relations and Eqs. (20-23). The equilibrium relations and the method used to determine $\partial C_j/\partial T'$ are presented in Appendix A. The determination of the quantity $\partial C_j/\partial C_{\tilde{i}}$ is not so straight forward and presents some difficulty. If one assumes that $\partial C_j/\partial C_{\tilde{i}} = 0$ for all j species which do not appear in the group for the i element (Table I), the gradients can also be determined from the equilibrium relation and Eqs. (20-23). By means of the analysis presented in Appendix A, the energy equation can be written as

$$\rho' \frac{r'}{r_w'}\left(u' \frac{\partial H'}{\partial x'} + \tilde{\kappa}\, v' \frac{\partial H'}{\partial y'}\right) = \frac{\partial}{\partial y'}\left[\frac{r'}{r_w'}\,\tilde{\kappa}\left\{\frac{\mu'}{P_r}\frac{\partial h'}{\partial y'} + \mu' \frac{\partial (u'^2/2)}{\partial y}\right.\right.$$

$$\left.\left. + \frac{\mu'}{P_r}\sum_{\tilde{i}=1}^{4}\sum_{j}(Le_j - 1)h_j \frac{\partial C_j}{\partial C_{\tilde{i}}}\frac{\partial C_{\tilde{i}}}{\partial y}\right\}\right] - \kappa' \frac{\partial}{\partial y'}(\mu' u'^2) - E'\tilde{\kappa}\frac{r'}{r_w'} \tag{39}$$

The energy equation is solved numerically in the same manner as the diffusion equation. The pertinent steps are indicated by Eqs. (32) to (36). The required boundary conditions are given by the value of the total enthalpy at the wall and at the shock. The wall enthalpy is assumed to be a known quantity.

Section 3

GAS PROPERTIES

3.1 NUMBER DENSITY AND THERMODYNAMIC PROPERTIES

A thermo-chemical equilibrium computer program (FEMP) was utilized to provide equilibrium compositions and thermodynamic properties for the gaseous mixtures as a function of enthalpy and pressure. For its operation, curve fits of the free energy function $-(F^{o}-E_{o}^{o})/RT$ and entropy S/R are supplied for each of the species that are to be considered (Ref. 11, 12). The equilibrium composition is then that one which gives the minimum free energy for the mixture at a given temperature and pressure. Once the species concentration of the mixture is known, the required thermodynamic properties of the mixture can then be computed using equations of classical thermodynamics.

The equilibrium composition for the nylon-phenolic pyrolysis products was investigated. At the lower temperatures ($2500^{o}K$, P = 1 ATM) an accurate representation is obtained by considering 15 species viz. C, C_2, H, H_2, N, N_2, O, O_2, CN, CO, C_2H, C_3H, C_4H, C_2H_2, and CHN. A comparison is shown in Fig. 2 between considering 15 and 41 species, respectively, for nylon phenolic. The same comparison is shown in Fig. 3; this time considering a 50% nylon phenolic, 50% air mixture.

At higher temperatures ($7000^{o}K$, P = 1 ATM) dissociation becomes more prominant and ionization occurs. The low temperature species no longer suffice to give an accurate description. For the range of temperatures above $7000^{o}K$, P = 1 ATM. that are of interest in this study, the important species to be considered now number twelve viz. C, C+, $\bar{e}$, H, H+, N, N+, O, O+, CN, CO, and

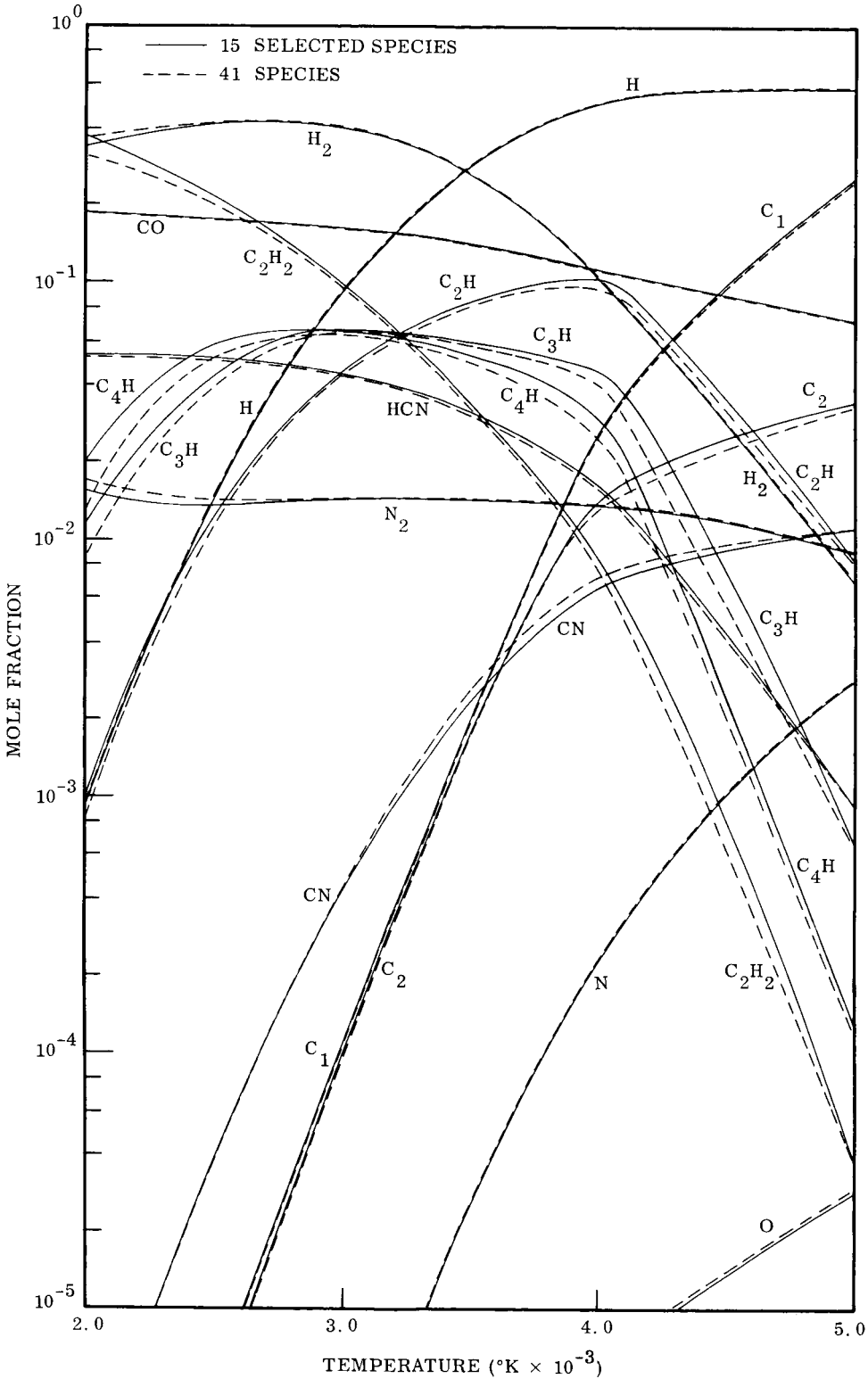

Fig. 2 Equilibrium Composition for Complete Pyrolysis of Nylon Phenolic 1 Atm Pressure

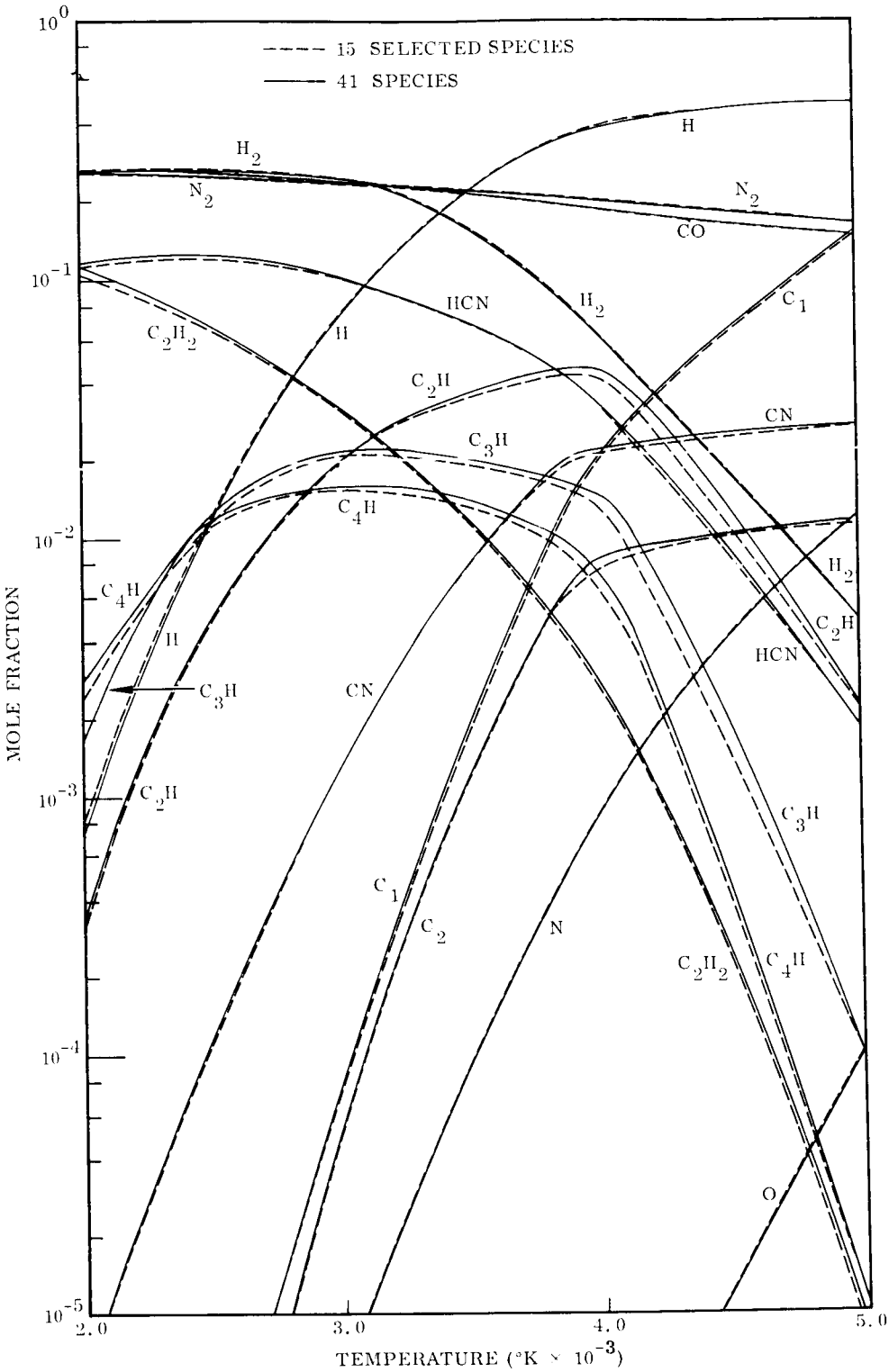

Fig. 3 Equilibrium Composition for Mixture of 50% by Mass of Air, and 50% by Mass of Nylon Phenolic 1 Atm Pressure

and N_2. Figures 4 and 5 depict the equilibrium composition at the higher temperatures. Since the shock layer will experience a large range of temperatures from the wall to the shock, there will be some portions of the layer described better by the low temperature species and some better by the high temperature species. The criterion used, to determine which of the sets of species is to be considered, is the compressibility of the gaseous mixture. The value of compressibility used is 1.5. At this value, the difference between equilibrium compositions of the major species, as predicted by using the two different sets of species, is less than 0.1 percent.

3.2 TRANSPORT PROPERTIES

Data from Refs. 13, 14 and 15 were used in specifying the viscosity and thermal conductivity for the individual neutral species. The following paragraph describes the methods used in these references.

The viscosity of an individual species was calculated by using the following formula (Ref. 16) which is a first approximation to an equation developed from kinetic theory

$$\mu_j = 1.794 \times 10^{-6} \frac{(M_j T)^{1/2}}{\bar{\Omega}^{(2,2)}_{j,j}} \left(\frac{\text{Lb}}{\text{ft-sec}}\right) \tag{40}$$

The collision integrals were obtained by using assumed potential-energy functions.

The thermal conductivity of a species is comprised of a translational portion, k_{TR}, and an internal portion, k_{INT}, representing the contribution due to the internal degrees of freedom. The translational part can be written in terms of the viscosity as

$$k_{INT} = \left(\frac{15}{4}\right) (R/M)\, \mu \tag{41}$$

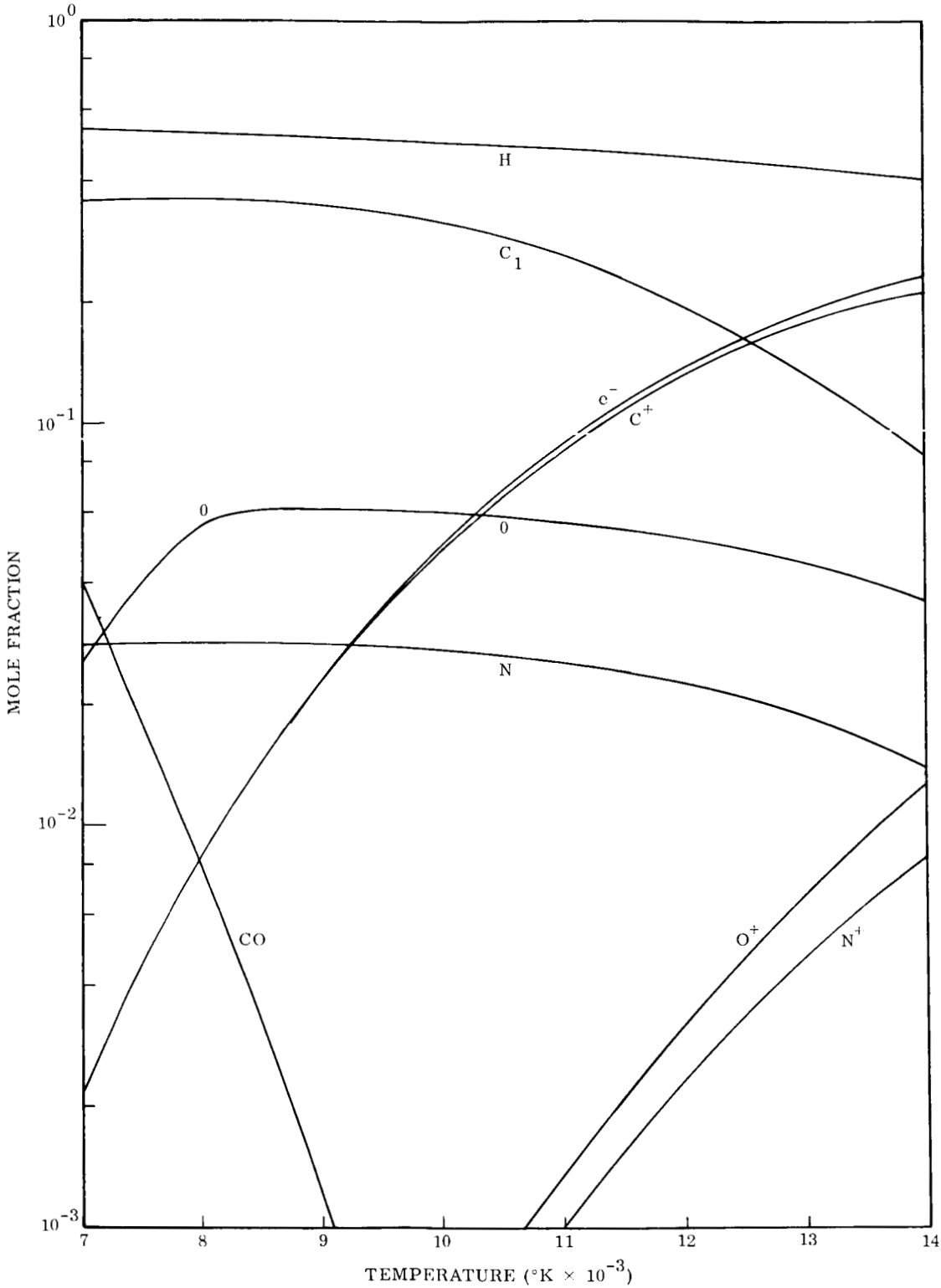

Fig. 4 Equilibrium Composition for Complete Pyrolysis of Nylon Phenolic 1 Atm Pressure

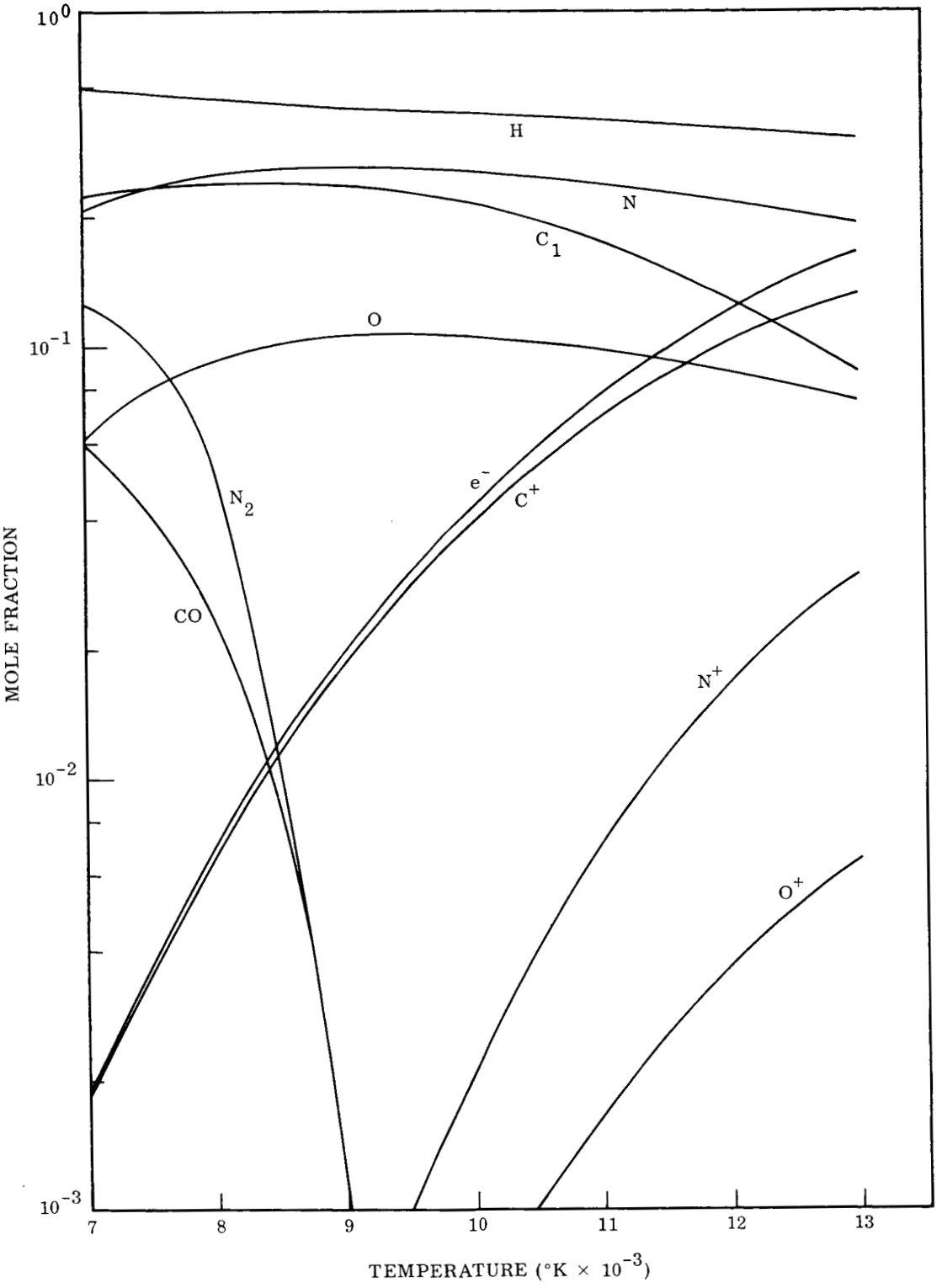

Fig. 5 Equilibrium Composition for Mixture of 50% by Mass of Air, and 50% by Mass of Nylon Phenolic 1 Atm Pressure

The internal portion of the thermal conductivity can be expressed by using an Eucken-type correction, i.e.

$$k_{INT} = k_{TR}\left(\frac{4}{15}\frac{C_v}{R}+\frac{8}{5}\right) \tag{42}$$

The diffusion coefficient is given in terms of the collision integrals for diffusion (Ref. 16).

$$D_{ij} = \frac{2 \times 10^{-6}\, T^{3/2}}{P\,\bar{\Omega}^{(1,1)}_{j,i}}\left[\frac{M_j + M_i}{M_j M_i}\right]^{1/2}\left(\frac{ft^2}{sec}\right) \tag{43}$$

The diffusion coefficients were adjusted so as to include the effect of considering an effective binary species. When realistic extremes of the molecular weights were tried for the effective binary species there was a small percentage difference in the effective diffusion coefficient. This occurs since the diffusion coefficient is inversely proportional to the square root of the reduced molecular weight, i.e. $D_{ji} \propto \left[M_j M_i / M_j + M_i\right]^{-1/2}$ which in turn is relatively insensitive to the value of M_i. The molecular weight of the effective binary species was then chosen to be the same as atomic oxygen (16) as a mean value. The polyatomics were assumed to have the same transport properties as the diatomics. For the ions, the equations described above were used with the necessary collision integrals being supplied by Ref. 17.

A cubic polynomial was used to curve fit these data for use in the computer program. These results are shown in Figs. 6, 7, and 8.

Ref. 18 gives approximate formulae and the rigorous kinetic theory formulation for transport properties of a mixture. As discussed in Ref. 18, the approximate formulae are quite accurate and consequently, are employed in the present analysis. The approximate formulae for viscosity and the frozen thermal conductivity are

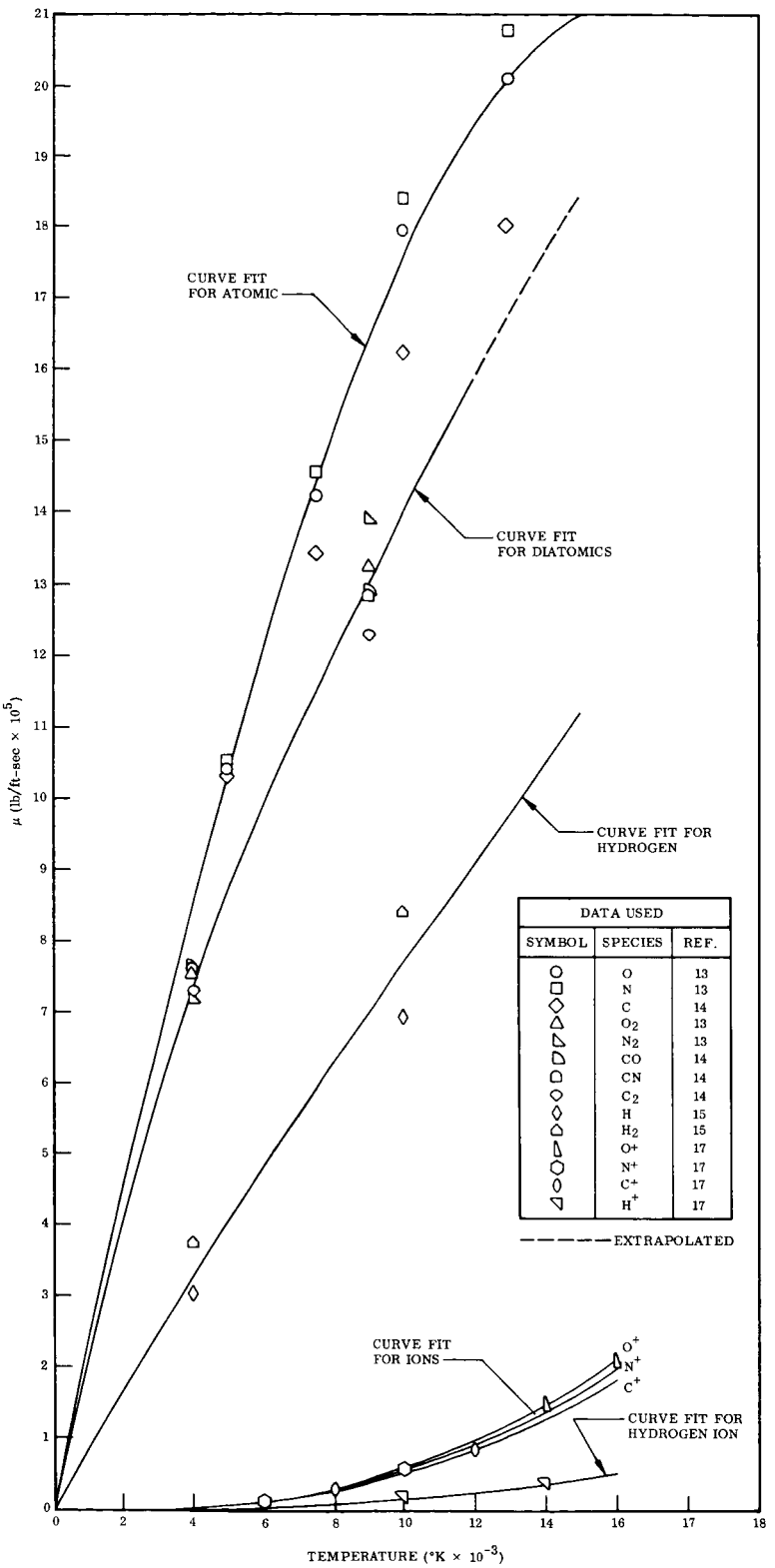

Fig. 6 Viscosity

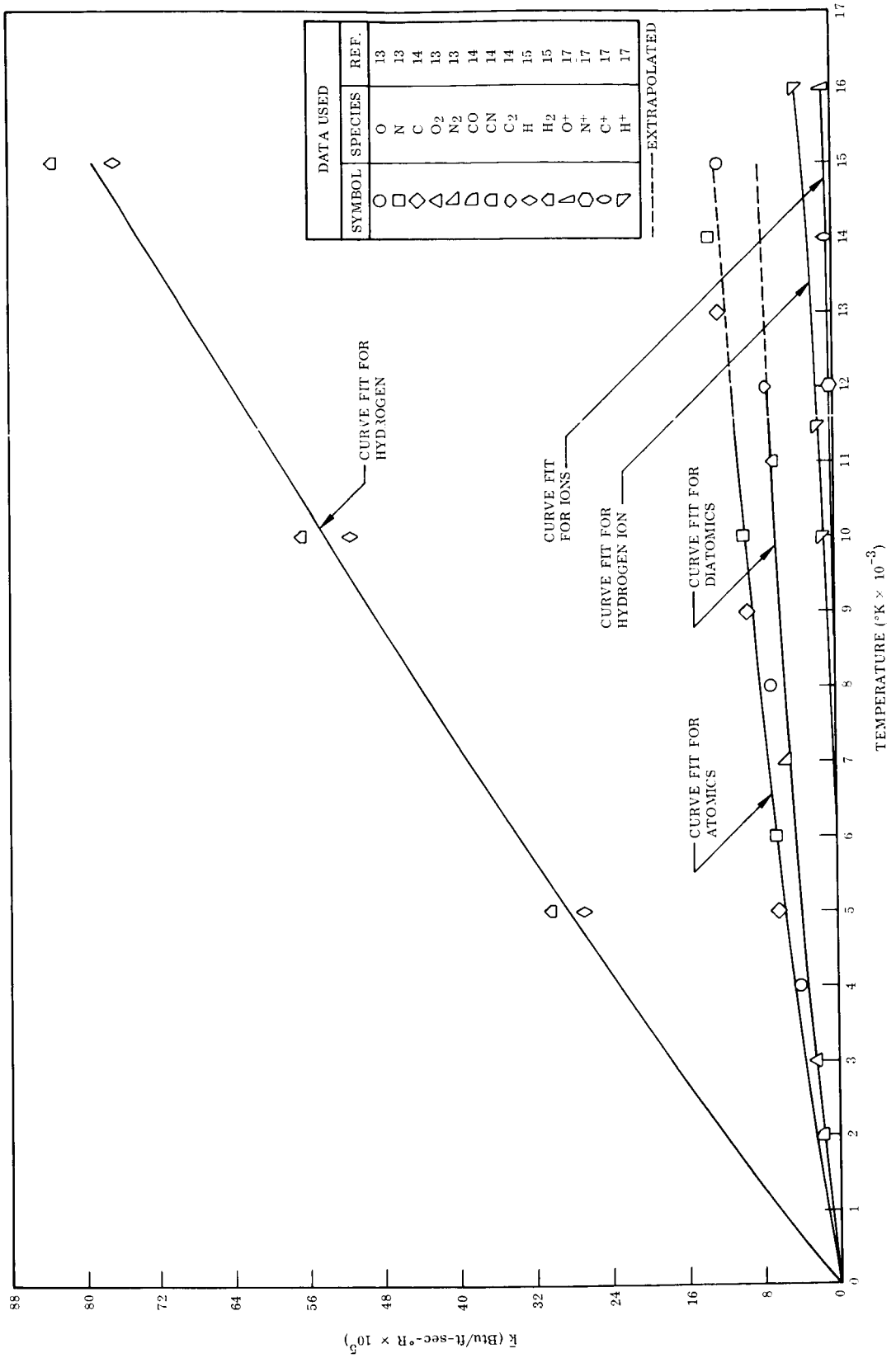

Fig. 7 Species Thermal Conductivity (Frozen)

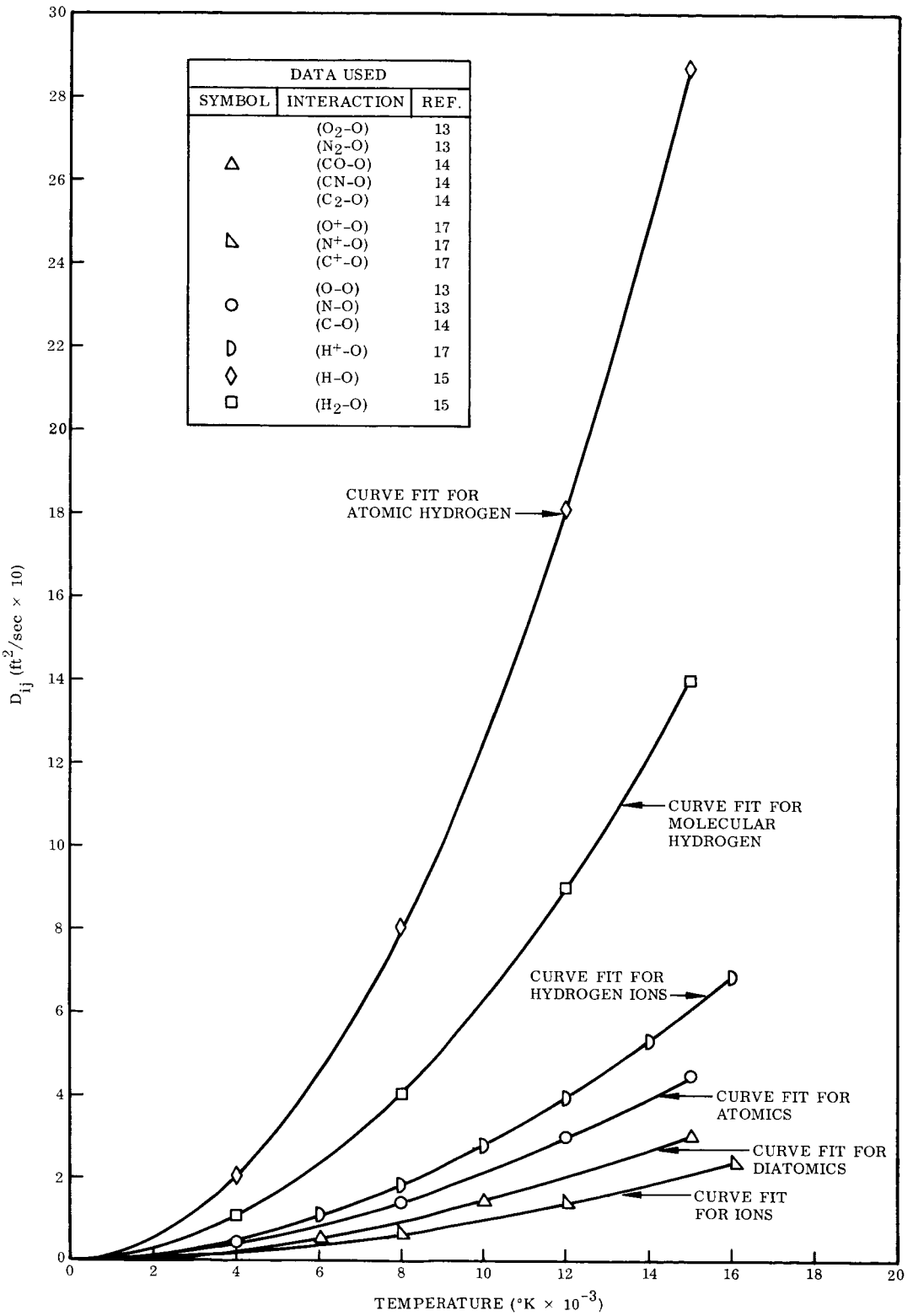

Fig. 8 Equivalent Binary Diffusion Coefficient at 1 Atm Pressure

$$\mu' = \sum_j \frac{C_j M_j'}{M_j'} \frac{1}{\sum_i \frac{C_i \phi_{ji}}{M_i'}} \qquad \phi_{ji} = \frac{\left[1 + \left(\frac{\mu_j'}{\mu_i'}\right)^{1/2} \left(\frac{M_i'}{M_j'}\right)^{1/4}\right]^2}{2\sqrt{2}\left(1 + \frac{M_j'}{M_i'}\right)^{1/2}}$$

$$\bar{k}' = \sum_j \frac{C_j \bar{k}_j'}{M_j'} \frac{1}{\sum \frac{C_i \phi_{ji}}{M_i'}} \qquad (44)$$

Fig. 9, taken from Ref. 17, shows a comparison of the Prandtl number of air obtained by using the above equations, with the results of Hansen (Ref. 19).

Section 4 describes an approximate version of the shock-layer solution, i.e., one which uses thermodynamic and transport properties of air in the solution of the diffusion equations. The curve fits given in Ref. 20 were used for this purpose.

3.3 ABSORPTION COEFFICIENTS

The radiative energy transfer within the shock layer depends critically on the absorption coefficient of the gas particles. The absorption coefficient is dependent on the nature of the gas particle, its number density, temperature, and the radiation frequency. The absorption coefficients utilized in the present analysis are summarized in Fig. 10. All of the important absorption coefficients summarized in Fig. 10 are given by simple analytical expressions in terms of the particle number density, temperature, and the radiation frequency. The expressions are used to evaluate the radiation flux gradient term in the energy equation.

The continuum absorption coefficients due to bound-free and free-free transitions for the neutral and singly ionized atoms of carbon, nitrogen, and oxygen were obtained from the theory of Biberman (Ref. 21) and Armstrong et al (Ref. 22). Biberman's results are used for the free-free and bound-free

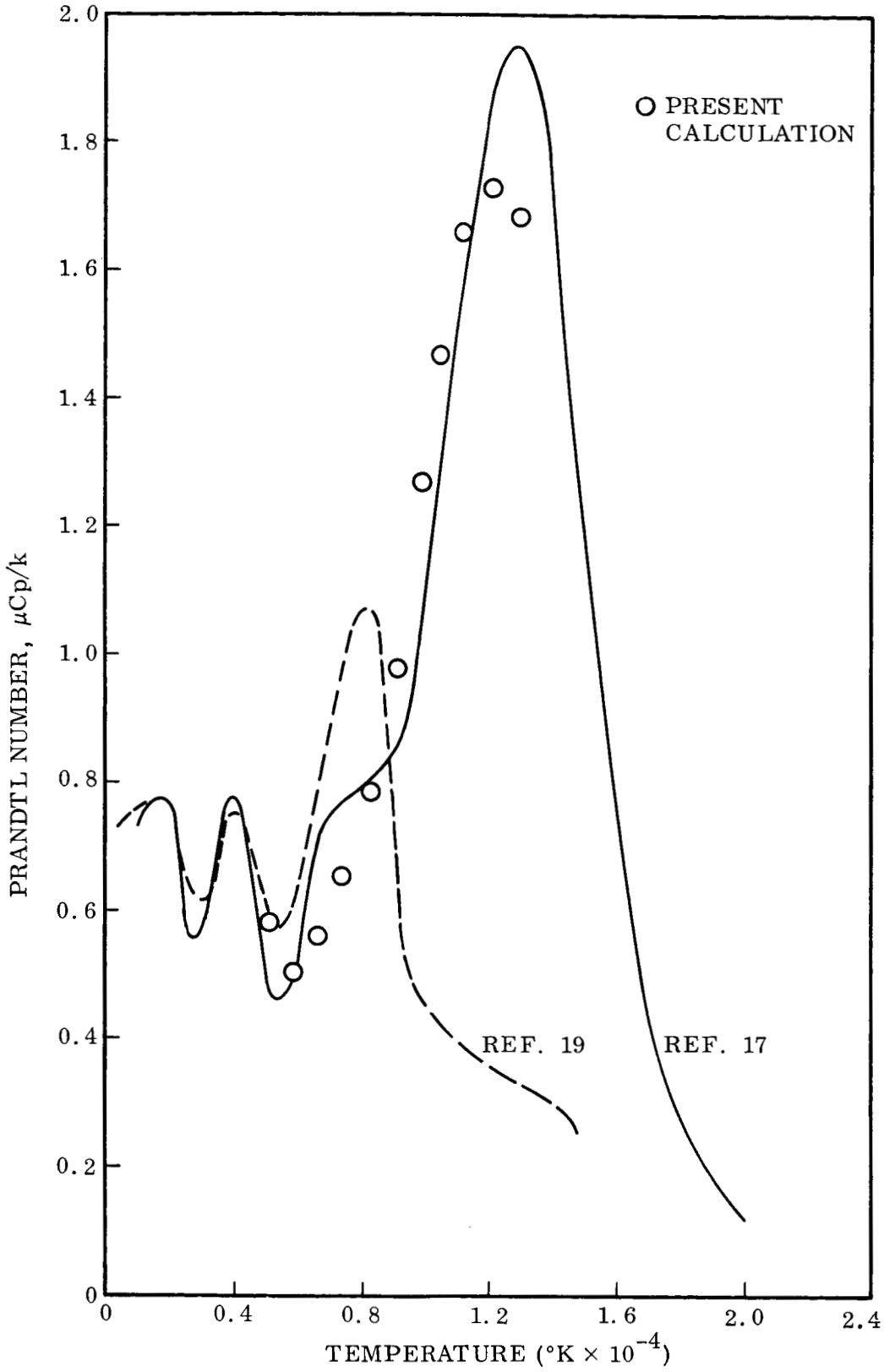

Fig. 9 Prandtl Number for Equilibrium Air at Atmospheric Pressure (Taken From Ref. 17)

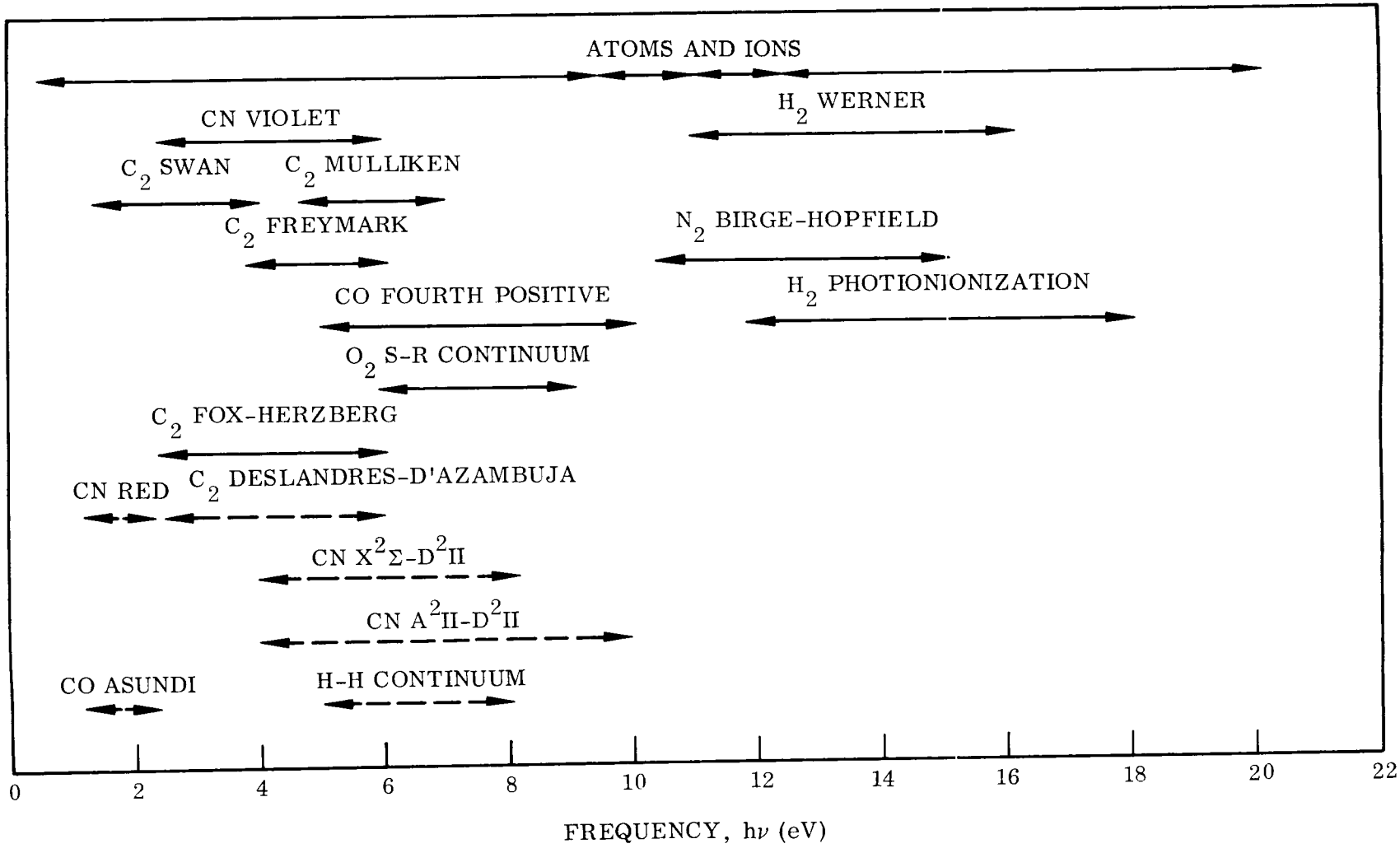

Fig. 10 Summary of Absorption Coefficients

transitions from the higher excited states while Armstrong's detailed quantum-mechanical calculations are used to provide cross-sections for photon absorption due to transitions from the ground and low lying excited states.

The absorption coefficient for the atoms and ions is written as the sum of the individual species absorption coefficients

$$\kappa_\nu(X) = \left[1 - e^{-X} \right]\left[(\kappa_\nu)_C + (\kappa_\nu)_N + (\kappa_\nu)_O + (\kappa_\nu)_{C^+} + (\kappa_\nu)_i\right] \quad (45)$$

where the term in the first bracket accounts for induced emission. The absorption coefficient of the oxygen ion is assumed to be equal to that of the nitrogen ion. This approximation is acceptable since these ions contribute little to the total absorption coefficient except at the higher frequencies where the radiation from the shock layer gas is likely to be blackbody.

An examination of the molecular absorption coefficients for air given in Refs. 23, 24, and 25 shows that the only important air molecular absorption coefficients in terms of absorbing radiant energy from the high temperature region are the O_2 Schumann-Runge continuum and the N_2 Birge-Hopfield band. The absorption coefficients for the various species are presented in Ref. (1) and in Appendix B.

A preliminary investigation was done to determine which of the molecular band systems and continua of the ablation products would be significant in absorping and emitting radiation. Table II gives the maximum equivalent absorption cross-section for each of the contributors of the ablation products.

TABLE II

Molecule	Contribution	Maximum Cross-Section CM^2	Comments
H_2	Werner	3×10^{-17}	3000°K results used
↓	H-H Continuum	5×10^{-22}	Omitted as being negligible
↓	Photoionization	7×10^{-18}	3000°K results used
C_2	Swan	3×10^{-17}	3000°K results used
↓	Deslandres-D'Azambuja	5×10^{-19}	Omitted as being negligible
↓	Fox Herzberg	4×10^{-18}	3000°K results used
↓	Mulliken	3×10^{-17}	3000°K results used
↓	Freymark	6×10^{-18}	6000°K results used
CN	Red	1×10^{-19}	Omitted as being negligible
↓	Violet	3×10^{-17}	3000°K results used
↓	A^2II-D^2II	4×10^{-20}	Omitted as being negligible
↓	X^2 -D^2II	5×10^{-20}	Omitted as being negligible
CO	Asundi	1×10^{-22}	Omitted as being negligible
↓	4th Positive	2×10^{-18}	6000°K results used

The absorption coefficients for molecular band systems of diatomic molecules present in the ablation products were computed using a "smeared line model" presented by Patch, Shackleford, and Penner (Ref. 26). In this model the average strength (the f-value) of a band is given by a continuous exponential distribution in frequency in which there is no distinction between the various branches of a given band. In cases where the lack of spectroscopic data precludes more detail, the average strength of a transition or groups of transitions is uniformly distributed over the pertinent spectral interval. The required Franck-Condon factor and f-values for the bands were taken from the

open literature (Refs. 27 through 49). A summary of transition strength taken from Ref. 50 is given in Table III.

TABLE III (From Ref. 50)

TRANSITION STRENGTHS

	Band System or Process	Spectroscopic Notation	f
H_2	Werner	$C^1\Pi_u \leftarrow X^1\Sigma_g^+$	0.4
↓	Photoionization	Cont. $\leftarrow X'\,\Sigma_g^+$	----
C_2	Swan	$A^3\Pi g \leftarrow X'^3\Pi_u$	0.029
|	Fox-Herzberg	$B^3\Pi g \leftarrow X'^3\Pi u$	0.05
|	Mulliken	$d^1\Sigma_u^+ \leftarrow X^1\Sigma_g^+$	0.10
↓	Freymark	$e^1\Sigma_g^+ \leftarrow b^1\Pi u$	0.02
CN	Violet	$B^2\Sigma^+ \leftarrow X^2\Sigma^+$	0.027
CO	Fourth Positive	$A^1\Pi \leftarrow X^1\Sigma^+$	0.017

The form of the equations used in Ref. 50 is

$$\sigma^*(\tilde{\nu},T) = \sum_{v',v''} \frac{\pi e^2}{mc^3} f_u q(v',v'') P(I'',v'') \frac{Be''}{\nabla B} \frac{hc}{kT} e^{-[\tilde{\nu}-G(v')-G(v'')]\frac{hc}{kT}} \qquad (46)$$

where

$\tilde{\nu}$ = wave number

f_{el} = electronic f-value

$q(v',v'')$ = Franck-Condon factor for the transition from the lower vibrational state v'' to upper vibrational state v'

$P(I'',v'')$ = Boltzmann fractional population of the v''-th vibrational level in the I''-th (lower) electronic state

$G(v')$, $G(v'')$ = vibrational term

Be'', ∇B = spectroscopic constants

The contribution of the given band system to the total absorption coefficient is given by

$$\mu(\tilde{\nu}) = N\sigma^{*}(\tilde{\nu},T) \tag{47}$$

According to Ref. 50 the molecular continua is difficult to treat in general, but since H_2 molecular photoionization contributes to the total absorption coefficient, the effect of $H_2 + h\nu \longrightarrow H_2^{+} + \bar{e}$ was included in the calculation. The assumption enlisted was that the cross section is a function only of the kinetic energy of the ejected electron. From Ref. 50 the total cross section of one H_2 molecule is written in the form

$$\sigma^{*}(\tilde{\nu},T) = \sum_{v'} \sum_{v''} P(I'' = 1,v'')\sigma(E) \tag{48}$$

The function $\sigma(E)$ is obtained from experimental measurement on H_2.

For use in the computer program the effective absorption cross-sections were curve-fit. From the range of temperatures for which results were available, the temperature which yielded the highest absorption coefficient for a particular band or continuum was used. This has the effect of giving a conservative estimate for the absorption effect of the ablation products. The curve fits are shown in Fig. 11.

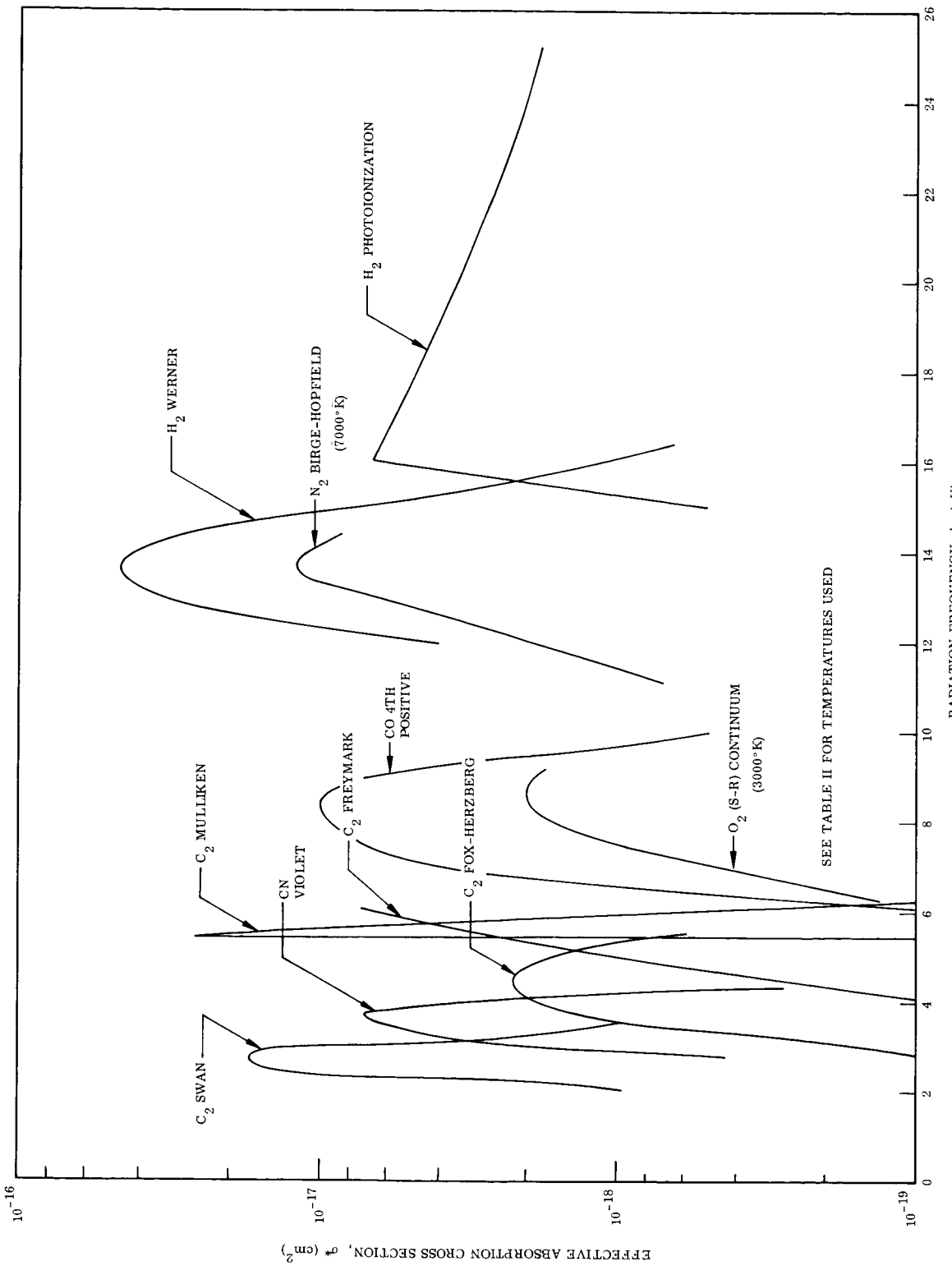

Fig. 11 Ablation Products Molecular Absorption

Section 4

NUMERICAL METHOD

The numerical solution to the conservation equation involves a rather complex iteration method. It is necessary to assume the value of several parameters in order to obtain a solution to the conservation equations. With the solution based on the assumed values, the accuracy of the initially assumed values can be checked. One can then iterate until satisfactory convergence is obtained.

At the stagnation point, a total enthalpy profile, the transformed standoff distance $\tilde{\delta}$, and the physical standoff distance δ are assumed. With these three quantities known, the appropriate boundary conditions, the velocity profile coefficients, a_i, and hence the velocity profile can be evaluated. At the stagnation point it is assumed that the shock is concentric with the body. Now the static enthalpy and the pressure variation across the shock layer can be evaluated. The three elemental species continuity equation are now solved by successive approximations (Eq. 36). With the above information, the assumed values of $\tilde{\delta}$ and δ can be checked by means of Eqs. (13-15). The solution is iterated until converged values for $\tilde{\delta}$ and δ have been obtained.

The energy equation can now be solved to obtain a new total enthalpy profile. The entire calculation procedure is repeated until all quantities have converged. The solution downstream of the stagnation point proceeds in a similar manner with the exception that the shock detachment distance, δ, is assumed to be a known function of the surface distance. Since δ is assumed known, one equation (Eq. 13) is not used in the downstream solution. This

equation is used a priori to obtain a new shock detachment distance. One can in principle, iterate on the shock shape to obtain the solution around the body.

The above mentioned iteration scheme requires about five minutes of Univac 1108 running time for each enthalpy iteration. It was reasoned that it was the many equilibrium calculations performed inside the $\tilde{\delta}$ and δ loops, i.e., those whose purpose was to determine thermodynamic and transport properties for use in the diffusion equations, that contributed excessively to the required running time. A study was made of using thermodynamic and transport properties of air inside this loop, which has the effect of relieving the burden of repetitive equilibrium calculations in the $\tilde{\delta}$ and δ cycle. The equilibrium calculations were still performed, but only when required for the radiative fluxes and properties in the energy equation. This is commensurate with the main purpose of this study which is to include realistic number densities in the radiation calculation. The time required for an enthalpy iteration was reduced to two minutes and the convective and radiative heat transfer agreed to within fifteen percent of their exact values, i.e., the values obtained when equilibrium gas properties are used throughout. What this approximate version amounts to is that the momentum and diffusion equations are solved using the properties of air, while the energy equation is solved using the properties of the equilibrium gas mixture. The use of exact thermodynamic and transport properties in the solution of the energy equation is desirable since this is the most crucial equation in the analysis.

Section 5

DISCUSSION OF RESULTS

The shock layer structure at the stagnation point of a nylon phenolic sphere with a nose radius of 1 ft. has been determined for a flight velocity of 41,000 fps and an altitude of 180,000 ft. The surface mass injection rate, $(\rho v)_w$ was taken to assume values up to 5% of the free stream mass flux, $(\rho U)_\infty$. Chemical reactions between the char and the shock layer gas have been omitted in these solutions. Surface chemical reactions will be included in additional solutions which will be obtained in the near future. Additional flight conditions will also be considered.

Velocity, enthalpy and elemental species concentration profiles are shown in Fig. 12 with and without mass injection. The decrease in the total enthalpy in the inviscid region of the shock layer is due to radiation cooling. The much larger gradient near the wall is, of course, due to viscous effects. The elemental species concentration profiles show that for the cases considered, the composition of the shock layer gas is almost identical to air. Species concentration profiles are shown in Fig. 13. The species not presented in Fig. 13 were omitted since their mass concentrations were too small to be included.

The monochromatic optical depth for several frequencies is presented in Fig. 14. These results show that the shock layer gas is highly absorbing in the vacuum ultraviolet ($h\nu \approx 13$ eV) and essentially transparent in the infrared ($h\nu \approx 1$ eV) and visible ($h\nu \approx 10$ eV) part of the spectrum. The corresponding monochromatic heat flux is presented in Fig. 15. An interesting feature of this figure is the behavior at $h\nu = 14.3$ eV. The ionization edge located at this frequency causes a step increase in the absorption coefficient which results in the gas behaving black at a distance closer to the surface. Due to the non-isothermal structure of the shock layer this location corresponds to a lower temperature. The gas radiating as a black body at this lower temperature results in a step decrease in the radiative heat flux to the surface.

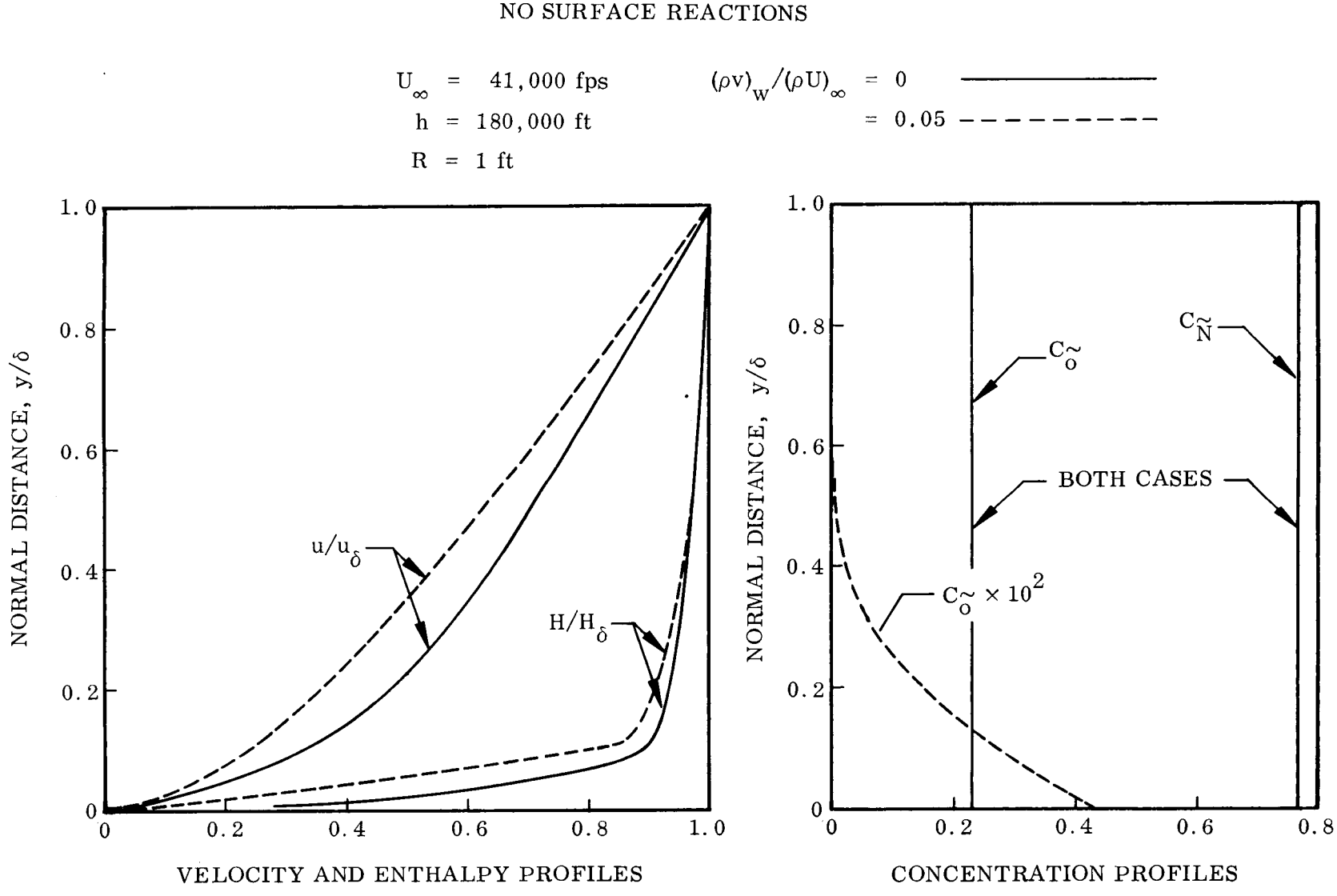

Fig. 12 Velocity, Enthalpy, and Elemental Species Concentration Profiles at the Stagnation Point

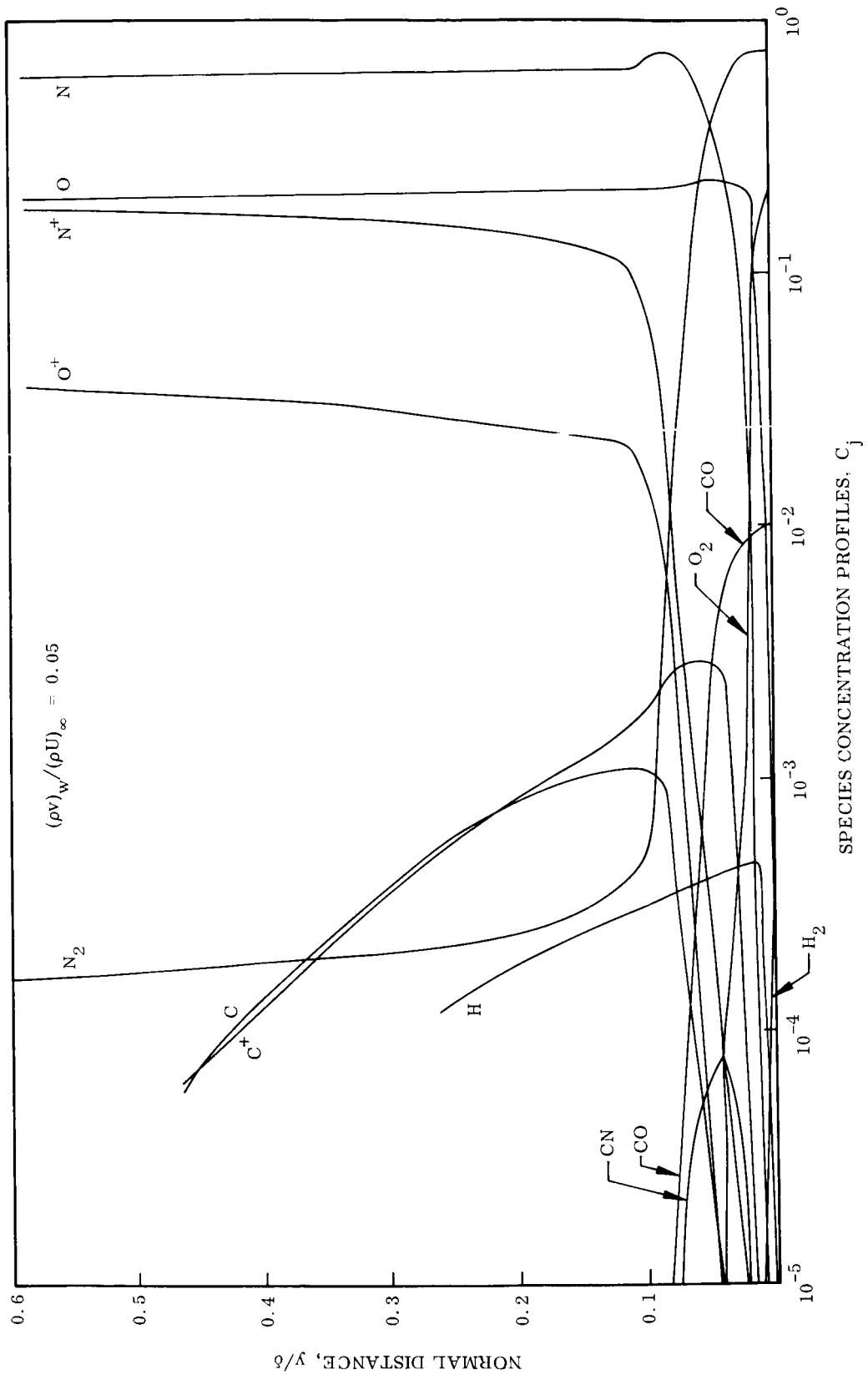

Fig. 13 Species Concentration Profiles (See Fig. 12 for Flight Conditions)

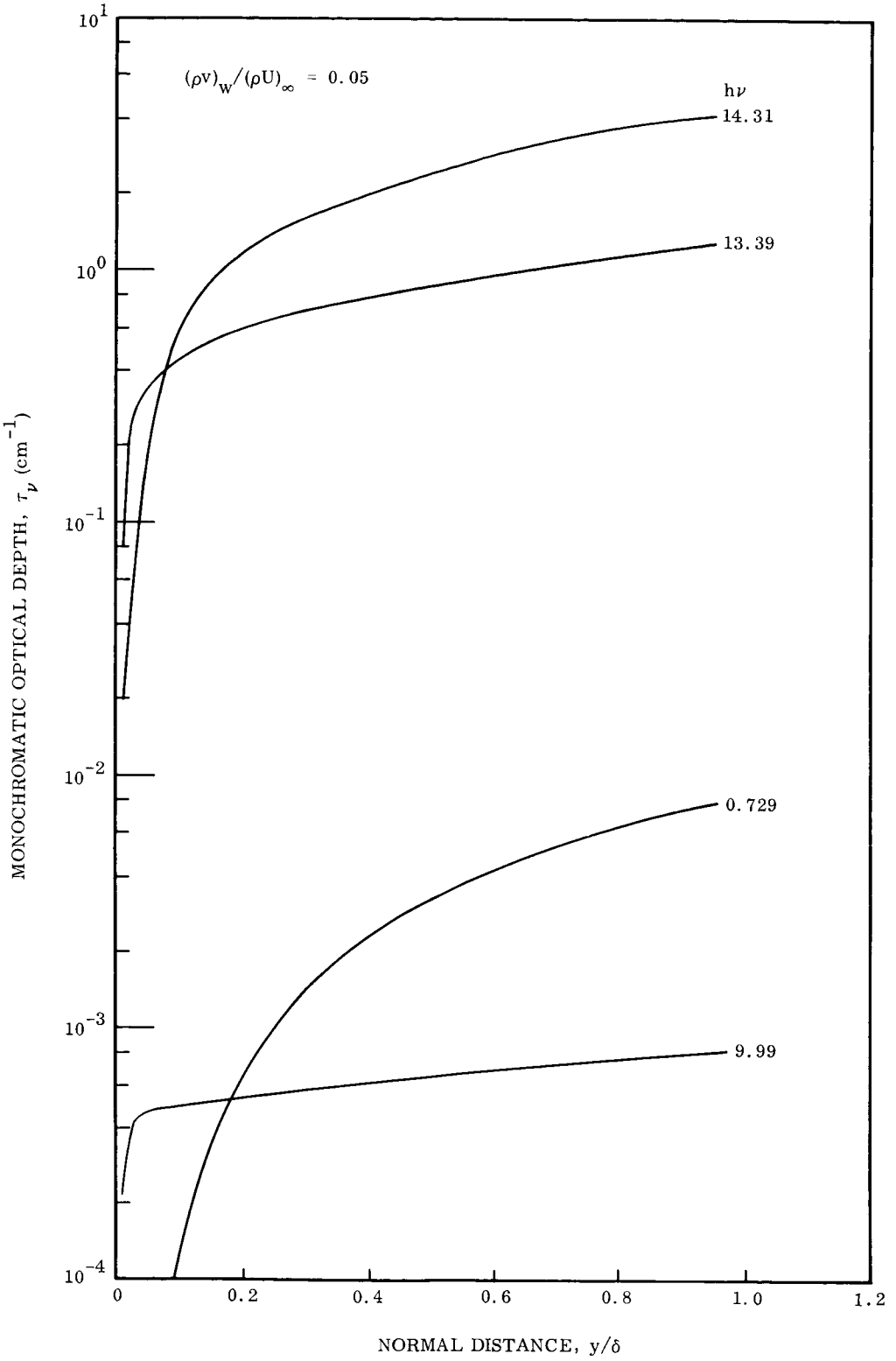

Fig. 14 Monochromatic Optical Depth (See Fig. 12 for Flight Conditions)

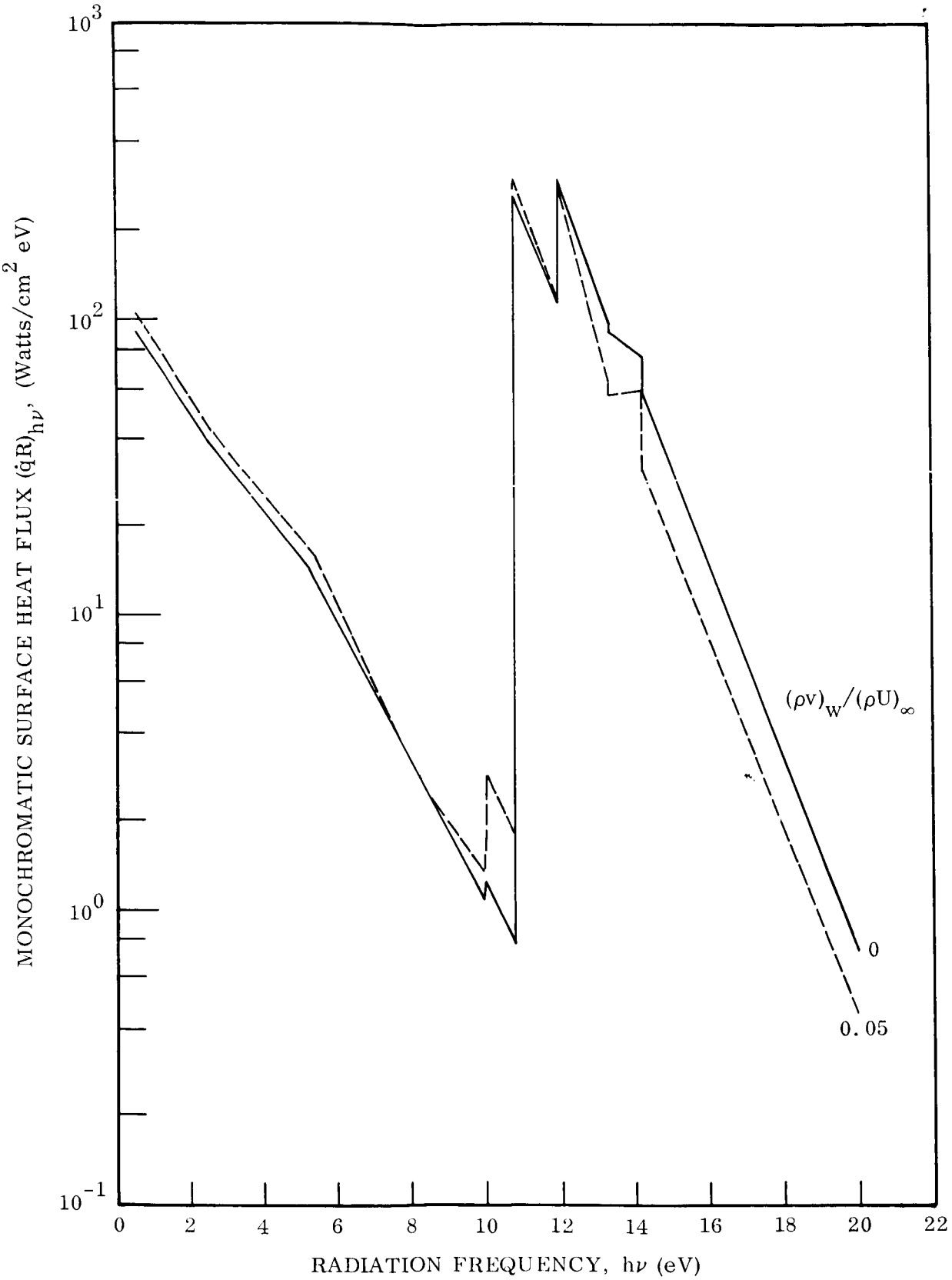

Fig. 15 Monochromatic Surface Heat Flux (See Fig. 12 for Flight Conditions)

Convective and radiative heat transfer results are presented in Table IV and Fig. 16.

Table IV

U_∞ = 41,000 ft/sec h = 180,000 ft R = 1 ft

	Boundary Layer Theory (Ref. 51)	Present Solution				
$\frac{(\rho v)_w}{(\rho U)_\infty}$	0	0	0.01	0.03	0.05	0.05**
$\delta/_R$	-	4.82×10^{-2}	5.04×10^{-2}	5.36×10^{-2}	5.71×10^{-2}	5.71×10^{-2}
q_c^*	1,800	1,979	1,443	634	209	206
q_R^*	-	795	804	763	755	757

* BTU/ft^2sec

** Neglecting the absorbing properties of the injected molecules

When mass in injected into the shock layer three separate effects influence the surface radiative heat flux: 1) an increase in shock layer thickness (sec Table IV) which tends to increase the flux, 2) a change in the temperature profile which indicates that more of the shock layer emits at a lower temperature which tends to decrease the flux, and 3) an addition of molecules in the vapor layer which absorb the incident radiation which tends to decrease the flux. For a 1% mass injection rate the net effect was to increase the radiative flux. For the higher mass injection cases, the net effect was to reduce the radiative flux. For the cases considered, however, the pyrolysis product vapor layers were too thin to significantly affect the radiative flux. Even at a 5% injection rate the reduction was less than 1% due to the absorbing properties of the vapor layer. Additional solutions for larger injection rates are currently being obtained.

The difference in the convective heating between the boundary-layer results of Ref. 51 and the present solution can be partially attributed to the different thermodynamic and transport properties utilized in the

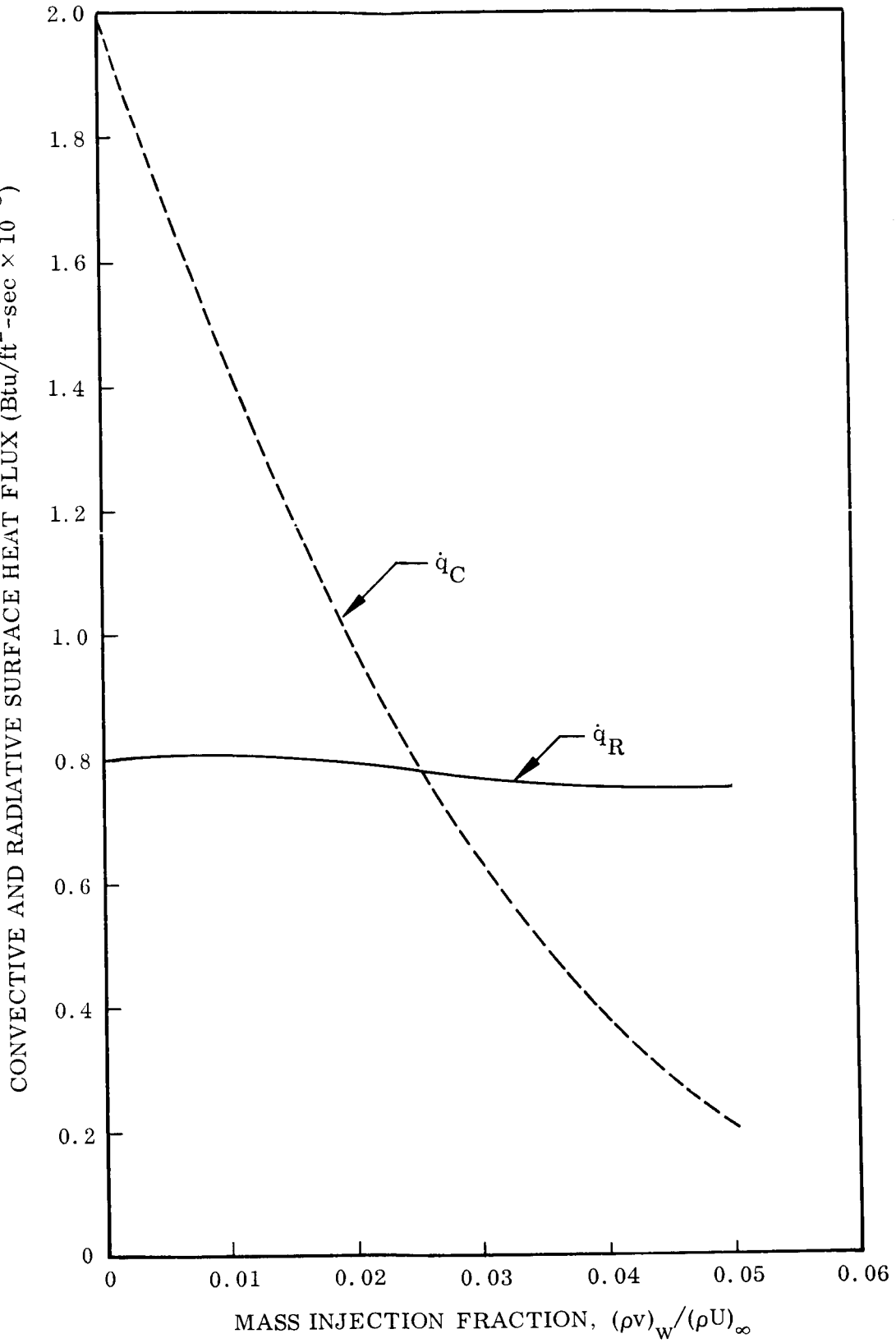

Fig. 16 The Effect of Mass Injection on Surface Heat Flux (See Fig. 12 for Flight Conditions)

respective solutions. The equilibrium property of air, as calculated by Hansen (Ref. 19) was employed in Ref. 51. Fig. 9 is a comparison of the total Prandtl numbers used in the respective solutions. The reduction in convective heating to the surface due to mass injection is demonstrated in Fig. 16.

Section 6

REFERENCES

1. Hoshizaki, H. and Wilson, K. H., "Convective and Radiative Heat Transfer During Superorbital Entry", LMSC Report No. 4-43-65-5, Lockheed Missiles & Space Co., November 1965, (Revised June 1966).

2. Scala, S. M., "The Equations of Motion in a Multicomponent Chemically Reacting Gas", Aerophysics Operation Research Memo. 5, General Electric Co., Missile and Ordnance Systems Dept., Philadelphia, Pennsylvania, (1957).

3. Hayes, W. D. and Probstein, R. F., Hypersonic Flow Theory, Academic Press, New York,(1959),pp. 388-389.

4. Kennet, H. and Strack, S. L., "Stagnation Point Radiative Transfer", ARS J. 31, No. 3, 370-372 (1961).

5. Koh, J. C. Y., "Radiation From Nonisothermal Gases to the Stagnation Point of a Hypersonic Blunt Body", ARS J. 32, 1374-1377 (1962).

6. Hoshizaki, H., "Some Aspects of Radiation Transfer During Hypervelocity Reentry , Proceedings of the Workshop on the Interdisciplinary Aspects of Radiation Transfer, Joint Inst. for Lab. Astro., Univ. of Colo., Vol. 11,(12 February 1965),p. 6.

7. Vincenti, W. G. and Kruger, C. H., Jr., Introduction to Physical Gas-dynamics, John Wiley & Sons, Inc., New York,(1965).

8. Smith, A. M. O. and Jaffe, N. A., "General Method for Solving the Laminar Nonequilibrium Boundary-Layer Equations of a Dissociating Gas", AIAA J. 4, No. 4, (1966).

9. Maslen, S. H. and Moeckel, W. E., "Inviscid Hypersonic Flow Past Blunt Bodies", J. Aerospace Sci. 24, No. 9, 683-693, (1957).

10. Lees, L., "Convective Heat Transfer with Mass Addition and Chemical Reactions", Combustion and Propulsion, Third AGARD Colloquium,(March 17-28, 1958), Palermo, Sicily.

11. Fickett, W. and Cowan, R. D., "Values of Thermodynamic Functions to 12,000°K for Several Substances", J. Chem. Phys. 23, p. 1349-1350, (1955).

12. Gilmore, F. R., "Equilibrium Composition and Thermodynamic Properties of Air to 24,000°K", Rand Report RM-1543, (1955).

13. Yun,Kwank-Sik, Weissman, S., and Mason, E. A., "High-Temperature Transport Properties of Dissociating Nitrogen and Dissociating Oxygen", Phys. Fluids 5, 672, (1962).

14. Lasher, L. E., "The Effect of Carbon Gas Injection (Graphite Ablation) on the Stagnation-Point Compressible Boundary Layer", Master Thesis, Cornell Univ., Ithaca, New York (1965).

15. Vanderslice, J. F., Weissman, S., Mason, E. A. and Fallon, R. J., "High-Temperature Transport Properties of Dissociating Hydrogen", Phys. Fluids 5, 155 (1962).

16. Hirschfelder, Curtiss, C. T., and Bird, R. B., Molecular Theory of Gases and Liquids, John Wiley & Sons, Inc., New York, (1954).

17. Yos, J. M., "Transport Properties of Nitrogen, Hydrogen, Oxygen, and Air to 30,000°K", AVCO RAD Technical Memorandum 63-7, (1963)

18. Brokaw, R. S., "Approximate Formulas for the Viscosity and Thermal Conductivity of Gas Mixtures", J. Chem. Phys. 29, 391-397, (1958).

19. Hansen, C. F., "Approximations for the Thermodynamic and Transport Properties of High-Temperature Air", NASA TR R-50, (1959).

20. Viegas, L. R. and Howe, J. T., "Thermodynamic and Transport Property Correlation Formulas for Equilibrium Air From 1,000°K to 15,000°K," NASA TN D-1429,(Oct. 1962).

21. Biberman, L. M. and Norman, G. E., "Recombination Radiation and Brehmstralung of a Plasma", J. Quant. Spec. Rad. Trans. 3, 221-245 (1963).

22. Armstrong, B. H., Brush, S., DeWitt, H., Johnston, R. R., Kelley, P. S., and Platas, O. R., "Opacity of High Temperature Air", Air Force Weapons Laboratory Report, AF WL-TR 65-17,(June 1965).

23. Churchill, D. R., Armstrong, B. H., and Mueller, K. G., "Absorption Coefficients of Heated Air: A Compilation to 24,000°K", AFWL TR-65-132, Vol. 1, Lockheed Missiles & Space Co.,(October 1965).

24. Evans, J. S. and Schexnayder, C. J., Jr., "An Investigation of the Effect of High Temperature on the Schumann-Runge Ultraviolet Absorption Continuum of Oxygen", NASA Technical Report R-92,(1961).

25. Allen, R. A., Textoris, A., and Wilson, J., "Measurements of the Free-Bound and Free-Free Continua of Nitrogen, Oxygen and Air", J. Quant. Spec. Rad. Trans. (January-February 1965).

26. Patch, R. W., Shackleford, W. L. and Penner, S. S., "Approximate Spectral Absorption Coefficient Calculations for Electronic Band Systems Belonging to Diatomic Molecules", J. Quant. Spec. Radiat. Transfer, Vol. 2,(1962), p. 263.

27. Nicholls, R. W., "Franck-Condon Factors to High Vibrational Quantum Numbers II: SiO, MgO, SrO, AlO, VO, NO", J. Res. NBS, Vol. 66A, (1962), pp. 227-231.

28. ----, "Laboratory Astrophysics", J. of Quantitative Spectroscopy and Radiative Transfer, Vol. 2, (1962), pp. 433-439.

29. ----, "Franck-Condon Factors to High Vibrational Quantum Numbers III: CN", J. Res. NBS, Vol. 66A, (1964), pp. 75-78.

30. Childs, D. R., Vibrational Wave Functions and Overlap Integrals of Various Band Systems, AVCO Corp., AVCO Research Report 147,(Jan. 1963).

31. Nicholls, R. W., "Franck-Condon Factors for the H_2 Lyman-Band System", Astrophysical Journal, Vol. 141, pp. 819-820, (1965).

32. Patch, R. W., "Vibrational Overlap Integrals for Ultraviolet Bands of H_2", J. Chem. Phys., Vol. 41, pp. 1881-1883, (1964).

33. Nicholls, R. W. et al., "Vibrational Transition Probabilities of Diatomic Molecules: Collected Results, IV -BeO, BO, CH^+, CO, NO, SH, O_2, O_2^+", Astrophysical Journal, pp. 399-406, (1959).

34. Jarmain, W. R., Fraser, P. A., and Nicholls, R. W., "Vibrational Transition Probabilities of Diatomic Molecules: Collected R sults, III - N_2, NO, O_2, O_2^+, OH, CO, CO^+", Astrophysical Journal, pp. 55-61, (1955).

35. Nicholls, R. W., "Franck-Condon Factors to High Quantum Numbers VI: C_2 Band Systems", J. Res. NBS, Vol. 69A, pp. 397-400, (1965).

36. Nicholls, R. W., Fraser, P. A., and Jarmain, W. R., "Transition Probability Parameters of Molecular Spectra Arising From Combustion Processes", Combustion and Flame, Vol. 3, pp. 13-38, (1959).

37. Jain, D. C., "Transition Probability Parameters of the Swan and Fox-Herzberg Band Systems of the C_2 Molecule , J. Quant. Spect. & Rad. Transfer, Vol. 4, pp. 427-440, (1964).

38. Robinson, D. and Nicholls, R. W., "Intensity Measurements in the O_2^+ Second Negative, CO Angstrom and Third Positive and NO and Molecular Band Systems", Proc. Phys. Soc., Vol. 71, p. 957, (1958).

39. Nicholls, R. W. et al, "Vibrational Transition Probabilities of Diatomic Molecules: Collected R sults, IV - BeO, BO, CH^+, CO, NO, SH, O_2, O_2^+, OH, CO, CO^+", Astrophysical Journal, Vol. 122, p. 55, (1955).

40. Jarmain, W. R., Fraser, P. A. and Nicholls, R. W., "Vibrational Transition Probabilities of Diatomic Molecules; Collected Results, III - N_2, NO, O_2, O_2^+, OH, CO, CO^+", Astrophysical Journal, Vol. 122, p. 55, (1955).

41. Wacks, Morton E., "Franck-Condon Factors for the Ionization of CO, NO and O_2", J. of Chem. Phys., Vol. 41, pp. 930-936, (1964).

42. Soshnikov, V. N., "Absolute Intensities of Electronic Transitions in Diatomic Molecules", Soviet Physics Uspekhi, Vol. 4, p. 425, (1961).

43. Clementi, Enrico, "Transition Probabilities for Low-Lying Electronic States in C_2", Astrophysical Journal, Vol. 132, pp. 898-904, (1960).

44. Allen, C. W., Astrophysical Quantities, University of London, Athlone Press, (1963).

45. Penner, S. S., Quantitative Molecular Spectroscopy and Gas Emissivities, Reading, Penn., Addison-Wesley, (1959).

46. Wentink, Jr., Tunis, et al., Electronic Oscillator Strengths of Diatomic Molecules, AVCO Corp., RAD-TM-64-33, (29 July 1964).

47. Anon., Venus-Mars Capsule Study, General Electric Missile & Space Div., GE 100(1), Vol. II, (1962).

48. United Aircraft Research Laboratories, Theoretical and Experimental Investigations of Spectral Opacities of Mixtures of Hydrogen and Diatomic Gases, RTD-TDR-63-1102, (Nov. 1963).

49. Bennett, R. G. and Dalby, F. W., "Experimental Oscillator Strength of the Violet System of CN", J. of Chem. Phys., Vol. 36, p. 399 (1962).

50. Creager, M. O., "Hardening Technology Studies - Volume III, Thermodynamics", LMSC B-13029, (1966).

51. Hoshizaki, H., "Heat Transfer in Planetary Atmospheres at Super-Satellite Speeds", ARS Journal, 1544-1552,(October 1962).

52. Butler, J. N. and Brokaw, R. S., "Thermal Conductivity of Gas Mixtures in Chemical Equilibrium", J. Chem. Phys. 26, 1636-1643, (1957).

53. G. E. Norman, "Photoionization Cross Section of the Lower Excited States and Oscillator Strengths of Certain Lines of Carbon and Nitrogen Atoms", Optics and Spectroscopy, Vol. XIV, No. 5 (1963).

54. D. R. Bate and M. J. Seaton, "The Quantal Theory of Continuous Absorption of Radiation by Various Atoms in Their Ground States", Mon. Notices, Roy. Astron. Soc., 109 (1949).

APPENDIX A

ENERGY FLUX FOR A MULTICOMPONENT GAS

The energy flux for a multicomponent reacting gas is given by (Ref. 52)

$$q' = -\bar{k}' \frac{\partial T'}{\partial y'} - \rho' \sum_j D_j' \; h_j' \frac{\partial C_j}{\partial y'} \tag{A-1}$$

where the effective binary mixture approximation has been employed.

The concentration of species j may be expressed as a function of the pressure, temperature, and the elemental concentrations. Noting that the pressure gradient is a second order effect and can be neglected, the species concentration gradient can be written as

$$\frac{\partial C_j}{\partial y'} = \frac{\partial C_j}{\partial T'}\bigg|_{P';\, C_{\tilde{i}}} \frac{\partial T'}{\partial y'} + \sum_{\tilde{i}=1}^{4} \frac{\partial C_j}{\partial C_{\tilde{i}}}\bigg|_{P';T'} \frac{\partial C_{\tilde{i}}}{\partial y'} \tag{A-2}$$

The energy flux then becomes

$$q' = -\left[\bar{k}' + \rho' \sum_j D_j' \; h_j' \frac{\partial C_j}{\partial T'}\right] \frac{\partial T'}{\partial y'} - \rho' \sum_{\tilde{i}=1}^{4} \sum_j D_j' h_j' \frac{\partial C_j}{\partial C_{\tilde{i}}} \frac{\partial C_{\tilde{i}}}{\partial y'} \tag{A-3}$$

In order to write the energy flux in terms of the static enthalpy gradient, consider the mixture enthalpy which is given by

$$h' = \sum_j C_j h_j' \tag{A-4}$$

It may be written in a functional form as

$$h' = h'(C_{\tilde{i}}, T') \tag{A-5}$$

Differentiating the enthalpy with respect to y gives

$$\frac{\partial h'}{\partial y'} = \frac{\partial h'}{\partial T'} \frac{\partial T'}{\partial y} + \sum_{\tilde{i}=1}^{4} \frac{\partial h'}{\partial C_{\tilde{i}}} \frac{\partial C_{\tilde{i}}}{\partial y} \tag{A-6}$$

From Eq. (A-4) we can obtain the following relationships

$$\frac{\partial h'}{\partial T'} = \sum_{j} C_j (C_p')_j + \sum h_j' \frac{\partial C_j}{\partial T}$$

$$\frac{\partial h'}{\partial T'} = \bar{C}_p' + \sum_{j} h_j' \frac{\partial C_j}{\partial T} \tag{A-7}$$

$$\frac{\partial h'}{\partial C_{\tilde{i}}} = \sum_{j} h_j' \frac{\partial C_j}{\partial C_{\tilde{i}}} \tag{A-8}$$

Substituting Eqs. A-7 and A-8 into Eq. A-6 yields

$$\frac{\partial h'}{\partial y'} = (\bar{C}_p' + \sum_{j} h_j' \frac{\partial C_j}{\partial T}) \frac{\partial T'}{\partial y'} + \sum_{\tilde{i}=1}^{4} \sum_{j} h_j' \frac{\partial C_j}{\partial C_{\tilde{i}}} \frac{\partial C_{\tilde{i}}}{\partial y} \tag{A-9}$$

Solving for the temperature gradient gives

$$\frac{\partial T'}{\partial y'} = \frac{1}{C_p'} \left[\frac{\partial h'}{\partial y'} - \sum_{\tilde{i}=1}^{4} \sum_{j} h_j' \frac{\partial C_j}{\partial C_{\tilde{i}}} \frac{\partial C_{\tilde{i}}}{\partial y} \right] \tag{A-10}$$

where we have defined C_p' to be

$$C_p' = \bar{C}_p' + \sum_{j} h_j' \frac{\partial C_j}{\partial T} \tag{A-11}$$

By means of Eq. (A-10), the energy flux becomes

$$q' = - \frac{k'}{C_p'} \left[\frac{\partial h'}{\partial y'} - \sum_{\tilde{i}=1}^{4} \sum_{j} h_j' \frac{\partial C_j}{\partial C_{\tilde{i}}} \cdot \frac{\partial C_{\tilde{i}}}{\partial y} \right] - \rho' \sum_{\tilde{i}=1}^{4} \sum_{j} D_j' h_j' \frac{\partial C_j}{\partial C_{\tilde{i}}} \cdot \frac{\partial C_{\tilde{i}}}{\partial y} \tag{A-12}$$

where

$$k' = \bar{k}' + \rho' \sum_j D_j' h_j' \frac{\partial C_j}{\partial T'} \tag{A-13}$$

Now, by defining a Prandtl and Lewis number by

$$P_r = \frac{C_p' \mu'}{k'} \tag{A-14}$$

$$Le_j = \frac{\rho' C_p' D_j'}{k'} \tag{A-15}$$

the energy flux can be written as

$$q' = - \frac{\mu'}{P_r} \left[\frac{\partial h'}{\partial y'} + \sum_{\tilde{i}=1}^{4} \sum_j (Le_j - 1) h_j' \frac{\partial C_j}{\partial C_{\tilde{i}}} \frac{\partial C_{\tilde{i}}}{\partial y'} \right] \tag{A-16}$$

To evaluate the concentration change with temperature, which appears in the definition of C_p' (A-11) and k'(A-13), the equilibrium relations are differentiated at constant pressure and elemental concentration. All the equilibrium reactions are considered to take the following form:

$$n_1 A_1 \rightleftharpoons n_2 A_2 + n_3 A_3 \tag{A-17}$$

where the A_j represent the species and n_j their stoichiometric coefficients. Writing the equilibrium constant for the reaction gives

$$K_p'(T') = \frac{P_{A_2}'^{n_2} P_{A_3}'^{n_3}}{P_{A_1}'^{n_1}} \tag{A-18}$$

where the P_j' are the partial pressures and $K_p'(T')$ is the equilibrium constant (only a function of temperature). Writing Eq. (A-18) in terms of mass fractions gives

$$C_{A_1} = \left\{ M'_{A_1} \left(\frac{C_{A_2}}{M_{A_2}} \right)^{\frac{n_2}{n_1}} \left(\frac{C_{A_3}}{M_{A_3}} \right)^{\frac{n_3}{n_1}} \right\} \left\{ \frac{(P'\tilde{M}')^{(n_2 + n_3 - n_1)/n_1}}{[K'_p(T)]^{1/n_1}} \right\} \quad \text{(A-19)}$$

The equilibrium constant is approximated as a function of temperature by the following equation

$$\log K'_p(T') = a' + b'/T' \quad \text{(A-20)}$$

where a' and b' are constants.

For the "low temperature" species there are seven independent equilibrium relations of the form of Eq. (A-19) and four elemental conservation equations of the form given by Eqs. (20-23). These eleven equations are used to describe the eleven species considered. For the "high temperature" species there are eight independent equilibrium relations of the form of Eq. (A-19) and four elemental conservation equations to describe the twelve species considered. These equations are differentiated with respect to temperature (at constant pressure and elemental concentration) to form a set of coupled equations for the required $\partial C_j/\partial T'$ derivatives in both the "low temperature" and "high temperature" regions.

Since there are elemental concentration gradients, the energy flux contains a term proportional to the rate of change of an individual species concentration with respect to the elemental concentrations. The assumption is made that, unless a species is contained explicitly in an elemental mass fraction, its derivative with respect to that elemental mass fraction is zero. For example, in the "low temperature" region, $\partial C_H/\partial C_{\tilde{N}}$ is taken to be zero while $\partial C_{HCN}/\partial C_{\tilde{N}}$ is not since the latter appears explicitly in the definition of $C_{\tilde{N}}$ while the former does not. The following table shows the species contained in the elemental mass fraction.

Table A-1

Element i	Species j	
	"Low Temperature"	"High Temperature"
$\tilde{C}$	C, C_2, C_N, CO, CHN	C, C+, CN, CO
$\tilde{H}$	H, H_2, CHN	H, H+
$\tilde{O}$	O, O_2, CO	O, O+, CO
$\tilde{N}$	N, N_2, CN, CHN	N, N+, N_2, CN

The equations defining the mass fractions, i.e. the summation of the j species entries for the i element in Table A-1, are differentiated with respect to the elemental mass fractions. This gives $\partial C_j/\partial C_{\tilde{i}}$, $\tilde{i}$ = O, N, C, H. For example, the expression for $\partial C /\partial C_{\tilde{C}}$ in the "low temperature" region is

$$1= \frac{\partial C_C}{\partial C_{\tilde{C}}} + \frac{\partial C_{C_2}}{\partial C_{\tilde{C}}} 2+ M_{C,CN} \frac{\partial C_{CN}}{\partial C_{\tilde{C}}} + M_{C,CO} \frac{\partial C_{CO}}{\partial C_{\tilde{C}}} + M_{C,CHN} \frac{\partial C_{CHN}}{\partial C_{\tilde{C}}} \qquad \text{(A-21)}$$

Through the equilibrium relations, i.e., Eq. (A-19), the C_j can be expressed in terms of four independent species. For the "low temperature" species the atoms are used as the independent species and for the "high temperature" species, the ions are used as the independent species. For example, the expression for C_{C_2} in the "low temperature" region is

$$C_{C_2} = \frac{(P'\tilde{M}')^{-1}}{K'_{p_{C_2}}(T')} M_{C_2} \left(\frac{C_C}{M_C}\right)^2 \qquad \text{(A-22)}$$

where C_C is considered to be the independent quantity. By differentiating the equilibrium relations (at constant pressure and temperature) the $\frac{\partial C_j}{\partial C_j'}$ may be formed where the prime indicates that the species is one of the four independent ones. For example Eq. (A-22) would give

$$\frac{\partial C_{C_2}}{\partial C'_C} = \frac{2C_{C_2}}{C'_C} \tag{A-23}$$

Eq. (A-21) may be manipulated to yield an explicit expression for $\frac{\partial C'_C}{\partial C_{\tilde{C}}}$

$$\frac{\partial C'_C}{\partial C_{\tilde{C}}} = \left\{ 1 + \frac{\partial C_{C_2}}{\partial C'_C} + M_{C,CN} \frac{\partial C_{CN}}{\partial C'_C} + M_{C,CO} \frac{\partial C_{CO}}{\partial C'_C} + M_{C,HCN} \frac{\partial C_{HCN}}{\partial C'_C} \right\}^{-1} \tag{A-24}$$

The required derivatives, $\partial C_j / \partial C_{\tilde{i}}$ for the remaining species may then be expressed in terms of $\partial C'_j / \partial C_{\tilde{i}}$, viz.,

$$\frac{\partial C_j}{\partial C_{\tilde{i}}} = \sum_j \frac{\partial C_j}{\partial C'_j} \frac{\partial C'_j}{\partial C_{\tilde{i}}} \tag{A-25}$$

APPENDIX B

ABSORPTION COEFFICIENTS

The absorption coefficients for the various species were obtained from Refs. (21) and (22) and are listed below for the indicated intervals. The relations for the air species are as follows:

$0 \leq h\nu \leq 4.22$

$$(\kappa_\nu)_N = 4.5\ \tilde{a}\ N_N\ \theta\ e^{-(X_N - X)}\ \frac{\xi_N}{(h\nu)^3} \tag{B-1}$$

$$(\kappa_\nu)_O = \frac{8}{9}\ \tilde{a}\ N_O\ \theta\ e^{-(X_O - X)}\ \frac{\xi_O}{(h\nu)^3} \tag{B-2}$$

$$(\kappa_\nu)_i = 1.33\ \tilde{a}\ N_i\ \theta\ e^{-(X_i - X)}\ \frac{\xi_i}{(h\nu)^3} \tag{B-3}$$

where $\tilde{a} = 7.25 \times 10^{16}\ cm^2\text{-}ev^2$

$X_N = 14.3/\theta$, $X_O = 13.4/\theta$, $X_i = 25.5/\theta$

$X = h\nu/kT = h\nu/\theta$

ξ_N, ξ_O, ξ_i = quantum-mechanical correction factor (Fig. B-1)

$4.22 \leq h\nu \leq 10.8$

$$(\kappa_\nu)_N = (\text{Eq. (B-1)})\, e^{(4.22/\theta - X)} \tag{B-4}$$

$$(\kappa_\nu)_O = (\text{Eq. (B-2)})\, e^{(4.22/\theta - X)} \tag{B-5}$$

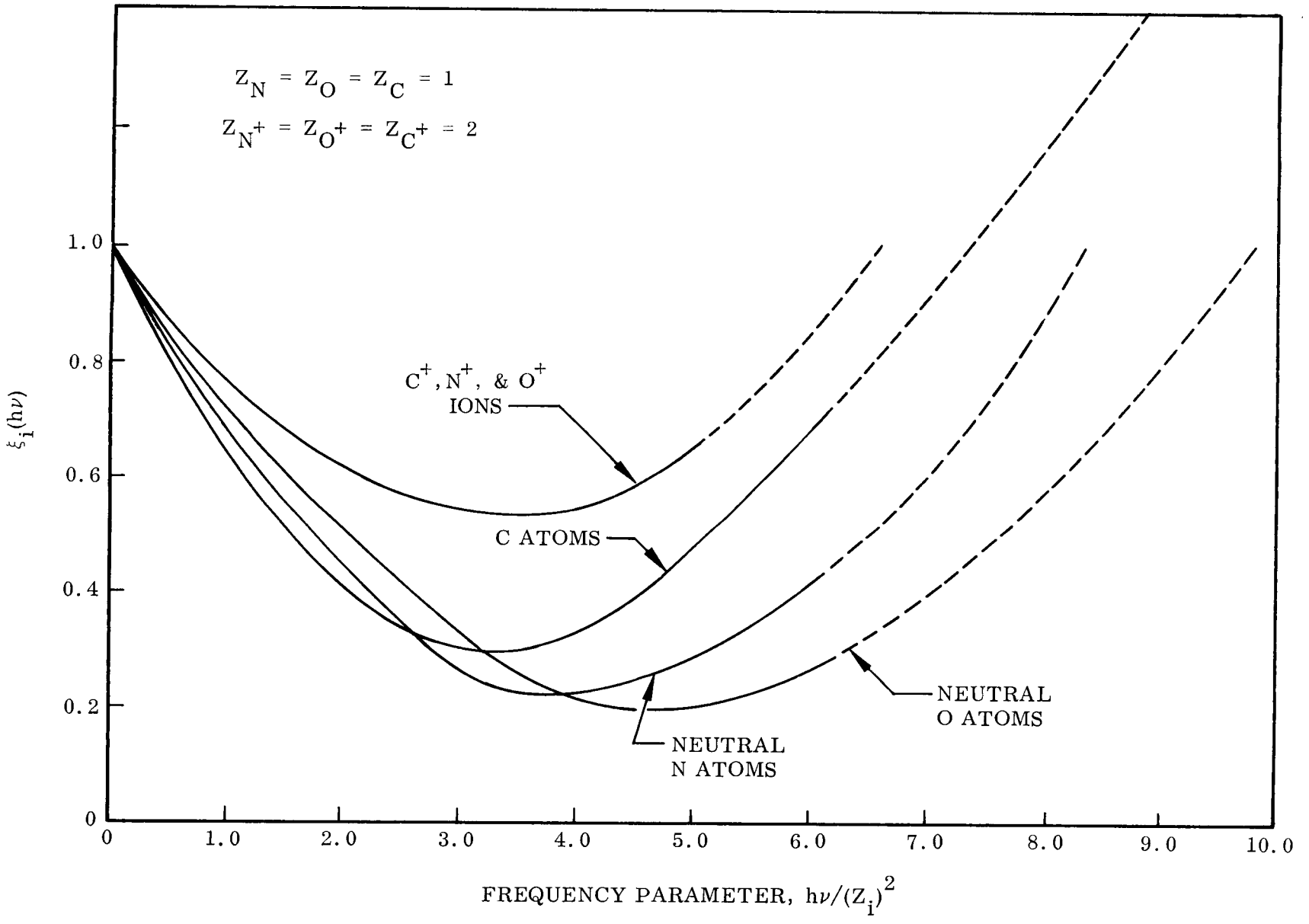

Fig. B-1 Quantum-Mechanical Correction Factor $\xi(h\nu)$

$$(\kappa_\nu)_i = (\text{Eq. (B-3)})$$

$10.8 \leq h\nu \leq 12.0$

$$(\kappa_\nu)_N = (\text{Eq. (B-4)}) + N_N \cdot \varphi_{N,1} \tag{B-6}$$

$$(\kappa_\nu)_O = (\text{Eq. (B-5)})$$

$$(\kappa_\nu)_i = (\text{Eq. (B-3)})\, e^{(11.2/\theta - \chi)} \tag{B-7}$$

$12 \leq h\nu \leq 13.4$

$$(\kappa_\nu)_N = (\text{Eq. (B-4)}) + N_N (\varphi_{N,1} + \varphi_{N,2}) \tag{B-8}$$

$$(\kappa_\nu)_O = (\text{Eq. (B-5)})$$

$$(\kappa_\nu)_i = (\text{Eq. (B-7)})$$

$13.4 \leq h\nu \leq 14.3$

$$(\kappa_\nu)_N = (\text{Eq. (B-8)})$$

$$(\kappa_\nu)_O = (\text{Eq. (B-5)}) + N_O \cdot \varphi_{O,1} \tag{B-9}$$

$$(\kappa_\nu)_i = (\text{Eq. (B-7)})$$

$14.3 \leq h\nu \leq 20$

$$(\kappa_\nu)_N = (\text{Eq. (B-4)}) + N_N (\varphi_{N,1} + \varphi_{N,2} + \varphi_{N,3}) \tag{B-10}$$

$$(\kappa_\nu)_O = (\text{Eq. (B-9)})$$

$$(\kappa_\nu)_i = (\text{Eq. (B-7)})$$

where

$$\varphi_{N,1} = 5.16 \times 10^{-17} \frac{e^{-(\chi_N - 10.8/\theta)}}{\left[4 + 10e^{-(2.38/\theta)} + 6e^{-(3.57/\theta)}\right]}$$

$$\varphi_{N,2} = 6.4 \times 10^{-17} \frac{e^{-(\chi_N - 12/\theta)}}{\left[4 + 10e^{-(2.38/\theta)} + 6e^{-(3.57/\theta)}\right]}$$

$$\varphi_{N,3} = 3.16 \times 10^{-17} \frac{1}{\left[4 + 10e^{-(2.38/\theta)} + 6e^{-(3.57/\theta)}\right]}$$

$$\varphi_{O,1} = 3.6 \times 10^{-17} \frac{1}{\left[9 + 5e^{-(1.98/\theta)} + e^{-(4.18/\theta)}\right]}$$

The absorption coefficients for molecular oxygen Schumann-Runge continuum were obtained from the results of Evans and Schexnayder (Ref. 24) In Ref. 24 the authors discuss the approximate formula of Sulzer-Wieland and point out its deficiency at elevated temperatures ($T \approx 10{,}000^{\circ}K$). At lower temperatures where the molecular oxygen is present in a gas mixture in chemical equilibrium, the approximate results of Sulzer-Wieland given below are adequate for present purposes.

$$\kappa_\nu = 1.49 \times 10^{-17} N_{O_2} \left[\tanh\left(\frac{0.0975}{\theta}\right)\right]^{1/2} \exp\left[-\tanh\left(\frac{0.0975}{\theta}\right) \times \left(\frac{h\nu - 8.56}{0.805}\right)^2\right] \quad \text{(B-11)}$$

The absorption coefficient for the nitrogen Birge-Hopfield band was obtained from results of R. Allen (Ref. 25). The cross section for $T = 7000^{\circ}K$ was approximated and used to obtain the following expression for the absorption

coefficient.

$$\kappa_\nu = 1.2 \times 10^{-17} N_{N_2} \exp\left[- \left|h\nu - 13.6 + \left(1 - \frac{0.603}{\theta}\right)\right|^{1.3}\right] \qquad \text{(B-12)}$$

The effective cross sections, defined by

$$\sigma^* = \frac{\kappa_\nu}{N} \qquad \text{(B-13)}$$

for the two molecules discussed above are presented in Fig. 11.

The continuum absorption coefficients for neutral and singly ionized carbon atoms were determined from a method similar to that used for nitrogen and oxygen atoms. Biberman's theory was used to calculate the free-free contribution and the free-bound contributions from the higher excited states. Photoionization cross-sections resulting from detailed quantum-mechanical calculations were available for the low lying excited states, Ref. (53), and ground state of neutral carbon, Ref. (54). The absorption coefficients for various frequency intervals are listed below.

$0 \leq h\nu \leq 3.78$

$$(\kappa_\nu)_C = 1.33\, \tilde{a}\, N_C\, \theta\, e^{-(\chi_C - \chi)} \frac{\xi_C}{(h\nu)^3} \qquad \text{(B-14)}$$

$$(\kappa_\nu)_{C^+} = 1.33\, \tilde{a}\, N_{C^+}\, \theta\, e^{-(\chi_C - \chi)} \xi_{C^+}/(h\nu)^3 \qquad \text{(B-15)}$$

$3.78 \leq h\nu \leq 7.08$

$$(\kappa_\nu)_C = 1.33\, \tilde{a}\, N_C\, \theta\, e^{-(\chi_C - 3.78/\theta)} \frac{\xi_C}{(h\nu)^3} \qquad \text{(B-16)}$$

$(\kappa_\nu)_{C^+}$ = (Eq. (B-15))

$7.08 \leq h\nu \leq 8.51$

$$(\kappa_\nu)_C = \text{Eq. (B-14)} + N_C \varphi_{C,1} \qquad \text{(B-17)}$$

$$(\kappa_\nu)_{C+} = \text{(Eq. (B-15))}$$

$8.51 \leq h\nu \leq 10$

$$(\kappa_\nu)_C = \text{(Eq. (B-14))} + N_C(\varphi_{C,1} + \varphi_{C,2}) \qquad \text{(B-18)}$$

$$(\kappa_\nu)_{C+} = \text{(Eq. (B-15))}$$

$10 \leq h\nu \leq 11.26$

$$(\kappa_\nu)_C = \text{(Eq. (B-14))} + N_C(\varphi_{C,1} + \varphi_{C,2} + \varphi_{C,3}) \qquad \text{(B-19)}$$

$$(\kappa_\nu)_{C+} = \text{(Eq. (B-15))}$$

$11.26 \leq h\nu \leq 14.88$

$$(\kappa_\nu)_{C+} = \text{(Eq. (54))} + N_C(\varphi_{C,1} + \varphi_{C,2} + \varphi_{C,3} + \varphi_{C,4}) \qquad \text{(B-20)}$$

$$(\kappa_\nu)_{C+} = \text{(Eq. (B-15))}$$

$14.88 \leq h\nu \leq 18.85$

$$(\kappa_\nu)_C = \text{(Eq. (B-20))}$$

$$(\kappa_\nu)_{C+} = 1.33\, \tilde{a}\, N_{C+}\, \theta\, e^{-(x_{C+} - 14.88/\theta)}\, \frac{\xi_{C+}}{(h\nu)^3} \qquad \text{(B-21)}$$

$h\nu > 18.85$

$$(\kappa_\nu)_C = \text{(Eq. (B-20))}$$

$$(\kappa_\nu)_{C+} = \text{(Eq. (B-21))} + N_{C+}\, \varphi_{C+,1}$$

where

$$\chi_C = 11.26/\theta \; ; \; \chi_{C+} = 24.4$$

ξ_{C+}, ξ_C = quantum-mechanical correction factor (Fig. B-1)

$$\varphi_{C,1} = 5 \times 10^{-17} \frac{e^{-(\chi_C - 7.08/\theta)}}{\Sigma_C}$$

$$\varphi_{C,2} = 2.2 \times 10^{-17} \frac{e^{-(\chi_C - 8.51/\theta)}}{\Sigma_C}$$

$$\varphi_{C,3} = 8.5 \times 10^{-17} \frac{e^{-(\chi_C - 10/\theta)}}{\Sigma_C}$$

$$\varphi_{C,4} = 9.9 \times 10^{-17} \frac{1}{\Sigma_C}$$

$$\varphi_{C+,1} = 6.8 \times 10^{-17} \frac{e^{-(\chi_C - 18.5/\theta)}}{\Sigma_{C+}}$$

$$\Sigma_C = 9 + e^{-2.68/\theta} + 5(e^{-1.265/\theta} + e^{-4.18/\theta})$$

$$\Sigma_{C+} = 6 + 12\, e^{-5.33/\theta}$$